

Utrecht University Repository

Title	Coherent J/ψ photoproduction at midrapidity in Pb–Pb collisions at $\sqrt{s_{NN}}=5.02$ TeV
Authors	ALICE Collaboration
Published in	Physics Letters, Section B: Nuclear, Elementary Particle and High-Energy Physics
Publication Date	2025-12
Link	https://dspace.library.uu.nl/handle/1874/480006
Citation	ALICE Collaboration 2025, 'Coherent J/ψ photoproduction at midrapidity in Pb–Pb collisions at $\sqrt{s_{NN}}=5.02$ TeV', Physics Letters, Section B: Nuclear, Elementary Particle and High-Energy Physics, vol. 871, 139952. https://doi.org/10.1016/j.physletb.2025.139952
Versions / License	Publisher version
Rights	https://www.uu.nl/en/university-library/license-and-reuse-conditions



Letter

Coherent J/ψ photoproduction at midrapidity in Pb – Pb collisions at $\sqrt{s_{NN}} = 5.02$ TeV

The ALICE Collaboration¹

ARTICLE INFO

Editor: Dr. M. Doser

Keywords:

Charmonium
Ultra peripheral heavy-ion collisions
Coherent photoproduction

ABSTRACT

The coherent J/ψ photoproduction cross section is measured for the first time at midrapidity in peripheral to semicentral Pb – Pb collisions at $\sqrt{s_{NN}} = 5.02$ TeV. The centrality differential cross section $d\sigma/dy$ is reported for the centrality range 40–90%, together with the doubly-differential cross section $d^2\sigma/dydp_T$, extracted in two peripheral centrality classes. The J/ψ mesons are reconstructed in the dielectron channel, in the rapidity interval $|y| < 0.9$ using the ALICE central barrel detectors. The J/ψ cross section at midrapidity is statistically compatible to the earlier ALICE measurement at forward rapidity and at the same centre-of-mass energy, and shows only a mild centrality dependence over the covered range. Several sets of theoretical calculations taking into account the hadronic overlap in the collisions but ignoring possible final-state effects from a hot expanding medium are found to give a fairly good description of the current measurements within uncertainties.

1. Introduction

In ultrarelativistic collisions between heavy ions, the Lorentz-contracted nuclei generate strong electromagnetic fields, and either of them can be treated as the source of a quasi-real photon, which interacts with the other nucleus treated as the target. The photoproduction cross section can be factorised as the product of the photon flux emanating from one of the colliding nuclei, which is proportional to the square of the nuclear electric charge, Z^2 , and the photonuclear cross section. This process can be viewed as a fluctuation of the photon into a quark-antiquark pair (colour dipole), which then interacts with the gluon field of the target nucleus, at leading order through the exchange of two gluons in a colour singlet state, producing a real vector meson [1]. In this approximation, the cross section is proportional to the square of the target gluon distribution at relevant values of (x, Q^2) [2]. The photoproduction can be either coherent, with the photon interacting with the target nucleus as a whole, generating a vector meson with very low transverse momentum ($\langle p_T \rangle \sim 60$ MeV/ c), or incoherent, with the photon interacting with a single nucleon, producing a meson of higher transverse momentum ($\langle p_T \rangle \sim 500$ MeV/ c) [3]. Photonuclear vector meson production is thus a powerful tool for investigating the gluonic structure of the target. Cross section measurements are sensitive to the gluon density in the nucleus and, due to the relatively low values of x that are accessible via this process, may constitute a probe for gluon shadowing or saturation. In addition, spatial characteristics of the gluon distribution, such as transverse size, shape, and fluctuations, can be accessed

through measurements of the differential cross section $d\sigma/dt$, with the Mandelstam variable $t \sim -p_T^2$ [4].

Photonuclear reactions have been most extensively studied in ultraperipheral collisions (UPCs) of heavy ions, taking place at impact parameters larger than the sum of their radii. With combinatorial and hadronic backgrounds being negligible, coherent and incoherent cross sections can readily be extracted. At the LHC energies, ALICE, CMS, and LHCb have studied coherent charmonium photoproduction in ultraperipheral Pb – Pb collisions at $\sqrt{s_{NN}} = 2.76$ TeV [5–7] and 5.02 TeV [4,8–12], in the rapidity ranges $|y| < 0.9$ (ALICE), $1.8 < |y| < 2.3$ (CMS, 2.76 TeV), $1.6 < |y| < 2.4$ (CMS, 5.02 TeV), $2.5 < y < 4$ (ALICE), and $2.0 < y < 4.5$ (LHCb). At the RHIC energies, the coherent and incoherent charmonium photoproduction cross sections in ultraperipheral Au-Au collisions at $\sqrt{s_{NN}} = 200$ GeV have recently been reported by STAR [13]. At both the LHC and RHIC, the measurements indicate a sizable suppression compared to the expectations from the impulse approximation. These observations are qualitatively reproduced by both gluon shadowing and gluon saturation phenomenological models, but none of them reproduce these data quantitatively over the entire covered Bjorken- x region.

Coherent photoproduction of J/ψ in heavy-ion interactions with nuclear overlap, manifesting as a prominent excess (for $p_T < 0.3$ GeV/ c) relative to the soft tail of the hadronically generated J/ψ spectrum, was first observed by ALICE in peripheral Pb – Pb collisions at $\sqrt{s_{NN}} = 2.76$ TeV and at forward rapidity ($2.5 < y < 4$), in the centrality range 30–90% [14]. The phenomenon was confirmed by STAR at RHIC energies, in Au – Au (20–80%) and U – U (40–80%) collisions at $\sqrt{s_{NN}} = 200$

Contact: alice-publications@cern.ch.

¹ Authors are listed at the end of this paper.

and 193 GeV, respectively, also presenting the p_T and $|t|$ dependence of the coherent cross section [15]. Recently, LHCb [16] and ALICE [17] reported a similar excess also in Pb – Pb collisions at $\sqrt{s_{NN}} = 5.02$ TeV, in both cases measured at forward rapidity ($2 < y < 4.5$ and $2.5 < y < 4$, respectively). LHCb, covering a range of peripheral collisions (approximately 65–90%), measured the differential J/ψ photoproduction yield dN/dy as a function of the number of participants ($\langle N_{part} \rangle$) and y , and the doubly-differential yield $d^2N/dydp_T$ as a function of p_T . ALICE extracted the coherent J/ψ photoproduction centrality differential cross section $d\sigma/dy$ over the centrality range 0–90%, setting an upper limit for the most central collisions (0–10%). A mild centrality dependence is revealed, compatible within uncertainties both with a flat trend and with a decrease of the cross section towards more central collisions.

The observation of coherent photoproduction in nuclear collisions with overlap inspired new theoretical developments [18–24], attempting to quantitatively describe the centrality, rapidity, and in the case of Refs. [20,21,24], the p_T dependence of the experimentally measured cross sections or yields. In order to account for the hadronic overlap, these models take the UPC picture as a baseline and impose geometric constraints implemented as impact parameter ranges, modifying the photon flux and, in some cases, also the photonuclear cross section.

Several questions remain unresolved regarding coherent photoproduction processes in a hadronic environment, including the roles of spectator and participant nucleons as photon sources and targets (theoretically explored in [20]), the survival of the coherence condition in the presence of nuclear breakup, and the time ordering of the hadro- and photoproduction. The coherent J/ψ p_T distribution, its impact parameter dependence, and the possible influence of destructive interference between the two photon sources and of the strong interactions in the nuclear overlap zone have been investigated in Refs. [20,21]. The shapes of the measured $|t|$ spectrum in Ref. [15] and p_T spectrum in Ref. [16] are well reproduced by these calculations within uncertainties. However, no available experimental data allow meaningful assessment of the evolution of p_T distributions with collision centrality.

An issue still sparsely explored by models is the potential influence of the hot and rapidly expanding partonic medium generated in the hadronic overlap zone on the coherently photoproduced, low- p_T charmonia. The latter are formed during the same narrow time interval as the initial hadronic interactions occur, presumably distributed over the surface of the target nuclei [23], and remain almost stationary in the transverse plane. This subset of the observable J/ψ population is uniquely identifiable as primordial survivors through their characteristic p_T distribution, and is, therefore, a particularly interesting QGP probe. Possible final-state medium effects are expected to be nearly absent in the most peripheral collisions, but may exhibit an onset with increasing nuclear overlap, manifesting as a reduction in measured cross sections and possibly a modulation in azimuthal distributions beyond that predicted by models considering only geometric constraints on photoproduction. Taking into account gluon-induced dissociation of charmonia in the plasma, Ref. [23] predicts a medium-induced suppression of the photoproduced J/ψ yield of ~ 20 –40% for semicentral collisions with $\langle N_{part} \rangle \sim 100$ –150.

This paper presents for the first time the J/ψ coherent photoproduction cross sections, measured at midrapidity in peripheral to semicentral (40–90%) Pb – Pb collisions at $\sqrt{s_{NN}} = 5.02$ TeV. The doubly-differential cross section $d^2N/dydp_T$ extracted by ALICE is reported for the first time for J/ψ photoproduction in collisions with nuclear overlap for two centrality classes, 50–70% and 70–90%. Section 2 gives an overview of the experimental apparatus and the data sample used, while Section 3 details the analysis and the extraction of systematic uncertainties. Section 4 presents the results and discusses them in the context of other existing J/ψ photoproduction measurements and relevant model calculations. Finally, Section 5 summarises the conclusions based on the LHC Run 2 data and points to opportunities offered by upcoming high-luminosity runs.

2. Experimental setup and data sample

A detailed description of the ALICE detector and its performance is provided in Refs. [25,26]. In this work, J/ψ mesons are reconstructed in the dielectron channel at midrapidity ($|y| < 0.9$), using the central barrel charged particle tracking detectors ITS (Inner Tracking System) [27] and TPC (Time Projection Chamber) [28] which provide very good tracking and electron identification in the pseudorapidity range $|\eta| < 0.9$. The ITS comprises six cylindrical detection layers based on different silicon technologies, surrounding the beam axis at radii ranging from 3.9 to 43 cm. The two innermost layers, requiring the highest granularity, are Silicon Pixel Detectors (SPD), while the two middle layers are Silicon Drift Detectors (SDD) and the two outermost ones are Silicon Strip Detectors (SSD). The ITS system is used for the determination of the event primary interaction point, precision tracking for the location of secondary vertices from weakly decaying particles, and event selection. The TPC is a cylindrical gaseous detector, filled with a mixture of argon and carbon dioxide, surrounding the ITS, with an inner radius of 0.85 m, an outer radius of 2.5 m, and a length of 5 m along the beam direction. It is the main tracking detector of the central barrel system, also performing particle identification based on the specific energy loss dE/dx in the gas.

In addition, a suite of detectors for global event characterisation is employed. The V0 detector [29] consists of two scintillating arrays covering the pseudorapidity ranges $2.8 < \eta < 5.1$ (VOA) and $-3.7 < \eta < -1.7$ (VOC), both being segmented in pseudorapidity and azimuthal angle. This subsystem is used for triggering and rejecting beam-induced background events, measuring charged particle multiplicity, and determining collision centrality and event plane azimuthal angle. The centrality in Pb – Pb collisions is defined as the percentile of the hadronic cross section corresponding to the charged particle multiplicity measured in the V0 detector [30]. A fit of a Glauber Monte Carlo model to the V0 amplitude distribution is used to relate the experimental centrality with geometric quantities like the average impact parameter ($\langle b \rangle$) and the number of participants ($\langle N_{part} \rangle$). The Zero Degree Calorimeter [31] comprises two sets of detector arrays located close to the beam axis on both sides of the nominal interaction point, at a distance of ± 112.5 m. Their tasks are detecting nucleons emitted at zero degree relative to the beam axis, aiding event characterisation both in hadronic and electromagnetic interactions, and rejection of beam-induced background.

The analysed data set was collected by ALICE during the 2015 and 2018 LHC Pb – Pb runs at $\sqrt{s_{NN}} = 5.02$ TeV. At midrapidity, data was acquired using the minimum bias (MB) trigger, defined by the coincidence of signals in both the VOA and VOC arrays. In the 2018 period, a central and a semicentral trigger were used in addition. These were defined using the MB trigger in combination with thresholds on the total online signal amplitude in the V0 detector, corresponding roughly to collision centralities of 0–10% and 30–50%, respectively. In this analysis, only events from the centrality range 40–90% were considered. Beam-induced background was rejected using timing information from the V0 and the Zero Degree Calorimeter detectors. All events were required to have a reconstructed primary vertex with a longitudinal position within ± 10 cm from the nominal interaction point. Events with pileup occurring during the TPC readout time were rejected in the offline analysis based on the correlation between the number of TPC and ITS (SDD + SSD) clusters. After all selections, the number of analysed events is approximately 37 million, 35 million, and 35 million for the 40–50%, 50–70%, and 70–90% centrality ranges, respectively. This corresponds to an integrated luminosity of $\sim 49.6 \mu\text{b}^{-1}$ for the 40–50% centrality interval and $\sim 24 \mu\text{b}^{-1}$ for both the 50–70% and 70–90% centrality intervals [32].

3. Data analysis

The J/ψ mesons are reconstructed using the e^+e^- decay channel. The selected electron candidates are good quality tracks reconstructed

through both the ITS and TPC, with a minimum momentum (p) of 1 GeV/ c and a pseudorapidity $|\eta| < 0.9$. To ensure excellent tracking quality, each track is required to have a minimum number of 70 associated space points in the TPC and a maximum calculated χ^2/N_{dof} value of 2 for the fit of the track to the clusters. Secondary particles are suppressed by requiring the maximum distance-of-closest-approach (DCA) of the track to the interaction vertex to be 1 cm in the transverse and 3 cm in the longitudinal direction. In addition, daughters of long-lived weakly decaying particles are removed using topological selections. In order to improve the tracking resolution and to reduce the number of secondary electrons from photon conversions in the detector material, at least one hit in either of the two SPD layers is required. Electrons and positrons are identified via their specific energy loss in the TPC gas by selecting a band of width $\pm 3\sigma_e$ around the electron expectation value estimated from a parameterisation of the measured average dE/dx as a function of momentum [33], with σ_e being the resolution of this measurement. To further reduce the contamination from hadrons, tracks with a dE/dx compatible with the pion or proton hypothesis within $\pm 3.5\sigma_{\pi/p}$, are rejected. Finally, electrons from photon conversions are further suppressed by using a prefiltering method [34] where candidate tracks forming a pair with invariant mass $m_{ee} < 50$ MeV/ c^2 when combined with a set of candidates selected using looser cuts, are excluded from the analysis.

In order to extract the yields of coherently photoproduced J/ψ , a two-dimensional distribution $N(m_{ee}, p_T)$ is constructed from all combinations of opposite-sign electron tracks from the same event and passing all selections described above. An unbinned 2-dimensional log-likelihood fitting procedure is applied to the measured distribution using a model which includes contributions from photoproduction ($F_{\text{phot},i}$), hadroproduction (F_{hadr}), and background (F_{bkg}):

$$F(m_{ee}, p_T) = f_{\text{bkg}} \cdot F_{\text{bkg}}(m_{ee}, p_T) + f_{\text{hadr}} \cdot F_{\text{hadr}}(m_{ee}, p_T) + f_{\text{phot}} \cdot \sum_i w_{\text{phot},i} F_{\text{phot},i}(m_{ee}, p_T), \quad (1)$$

where f_{bkg} , f_{hadr} , and f_{phot} are the normalisation parameters of the respective components, and $w_{\text{phot},i}$ are the fractional contributions from the different photoproduction processes, all described in more detail below.

The background component, F_{bkg} , is constructed as the sum of the combinatorial background and a much smaller background contribution from correlated semileptonic decays of heavy-quark pairs. The combinatorial background, $F_{\text{bkg}}^{\text{comb}}$, is constructed using the mixed-event technique, pairing opposite-sign electrons from events with similar global characteristics (centrality, vertex position, and event plane orientation). It is normalised using the like-sign pairs according to the expression

$$F_{\text{bkg}}^{\text{comb}}(m_{ee}, p_T) = N^{\text{ME-OS}}(m_{ee}, p_T) \cdot \frac{\sum_{m_{ee}, p_T} N^{\text{SE-LS}}(m_{ee}^i, p_T^i)}{\sum_{m_{ee}, p_T} N^{\text{ME-LS}}(m_{ee}^i, p_T^i)}, \quad (2)$$

where $N^{\text{ME-OS}}$ is the distribution of opposite-sign mixed-event pairs, while $N^{\text{SE-LS}}$ and $N^{\text{ME-LS}}$ are the like-sign pair distributions from the same and mixed events, respectively, summed over the m_{ee} and p_T . More details on the mixed-event procedure can be found in Ref. [35]. The two-dimensional correlated background component, $F_{\text{bkg}}^{\text{corr}}$, is constructed using a parameterisation of the residual background obtained from the (m_{ee}, p_T) dielectron distribution by subtracting the combinatorial background. The parameterisation is a 2D function which is factorisable into a first-order polynomial over the invariant mass dimension and a piecewise polynomial function over the p_T dimension. The correlated background component has a relatively small amplitude compared to the combinatorial background and to the J/ψ signal as well as to statistical fluctuations. The unbinned likelihood fit is therefore performed both with and without this component, yielding a small difference taken as a systematic uncertainty, as described later in this section. Due to the fact that $F_{\text{bkg}}^{\text{comb}}$ is already normalised via Eq. (2), $F_{\text{bkg}}^{\text{corr}}$ and the total sum

Table 1

Values of the χ^2/ndf for the invariant mass and p_T projections computed with respect to the fit model projections for the three analyzed centrality intervals.

Centrality	40–50%	50–70%	70–90%
Invariant mass projection (full fit range)	0.7	0.8	1.4
p_T projection ($p_T < 0.2$ GeV/ c)	1.6	1.9	1.1
p_T projection (full fit range)	1.6	1.6	1.3

F_{bkg} will also be normalised by construction, and the corresponding parameter f_{bkg} is therefore fixed in the fit of Eq. (1).

The two-dimensional hadroproduction component, F_{hadr} , is estimated via a Monte-Carlo simulation, described in more detail in Refs. [36,37]. This MC used a realistic kinematic distribution of inclusive unpolarised J/ψ based on existing measurements, including a fit to inclusive yields reported in Ref. [36]. The J/ψ were embedded in an underlying environment of Pb – Pb collisions generated using HIJING 1.0 [38]. The p_T shape of the embedded J/ψ signal was further tuned to match the p_T differential J/ψ yields recently measured by ALICE in the relevant centrality classes [37]. The J/ψ decay is forced into the dielectron channel using the PHOTOS package [39]. The simulated particles were transported through a model of the ALICE detector using GEANT3 [40], and then reconstructed with the same algorithms as used for real data.

The photoproduction component, $\sum_i w_{\text{phot},i} F_{\text{phot},i}$, is a sum of contributions from several processes, i , namely: coherent and incoherent J/ψ photoproduction, feed-down from coherently and incoherently photoproduced $\psi(2S)$, incoherent J/ψ photoproduction with nucleon dissociation, and continuum $\gamma\gamma \rightarrow e^+e^-$. These processes were simulated using the STARLight generator [41] with the same relative weights as those obtained in the UPC analysis reported in Ref. [9], and embedded into Pb – Pb collisions generated using the HIJING model with a similar setup as the one described for the hadronic component. Integrated in the range $p_T < 0.2$ GeV/ c , the ratio between the incoherent, feed-down and $\gamma\gamma$ continuum to the coherent J/ψ component is approximately 1%, 2.5% and 11%, respectively. The charmonia generated with STARLight are transversely polarised, as expected from s -channel helicity conservation and recently confirmed experimentally for coherently photoproduced J/ψ [42]. For the incoherent J/ψ with nucleon dissociation component, a process not incorporated in STARLight, the p_T shape was constructed using the H1 parameterisation [43]. The individual two-dimensional template shapes of the various processes, $F_{\text{phot},i}(m_{ee}, p_T)$, were obtained from the reconstructed electron pairs using the same reconstruction algorithm and analysis selections as for the data. The sum of all the reconstructed and weighted templates is used as a single component in the unbinned fit of Eq. (1) due to the fact that the size of the current data set does not allow the normalisation factors ($f_{\text{phot}} \cdot w_{\text{phot},i}$) of all these templates to vary independently in the fit.

In order to extract the signal, the unbinned data $N(m_{ee}, p_T)$ is fitted with the model from Eq. (1), where the only free parameters are f_{hadr} and f_{phot} . The fit is performed in the p_T range $0 < p_T < 7$ GeV/ c and the mass range $2 < m_{ee} < 4$ GeV/ c^2 . This procedure is performed in the centrality classes 40–50%, 50–70%, and 70–90%, and the raw yield of coherently photoproduced J/ψ , $N_{J/\psi, \text{coh}}$, is found by integrating the corresponding fitted template function for $p_T < 0.2$ GeV/ c and $2.92 < m_{e^+e^-} < 3.16$ GeV/ c^2 . The quality of the fitting procedure is illustrated in Fig. 1. The left panel shows a projection on the invariant mass dimension for candidate pairs with $p_T < 0.2$ GeV/ c for Pb – Pb collisions in the 70–90% centrality range. The right panel shows a projection on the p_T dimension for pairs in the invariant mass interval $2.92 < m_{e^+e^-} < 3.16$ GeV/ c^2 and the same centrality range. The two projections of the candidate pair distribution are compared to the projection from the fit model and its various components as described above.

The quality of the fit for the three analyzed centrality ranges was estimated quantitatively by calculating the χ^2/ndf for both the invariant mass and p_T projections and is listed in Table 1.

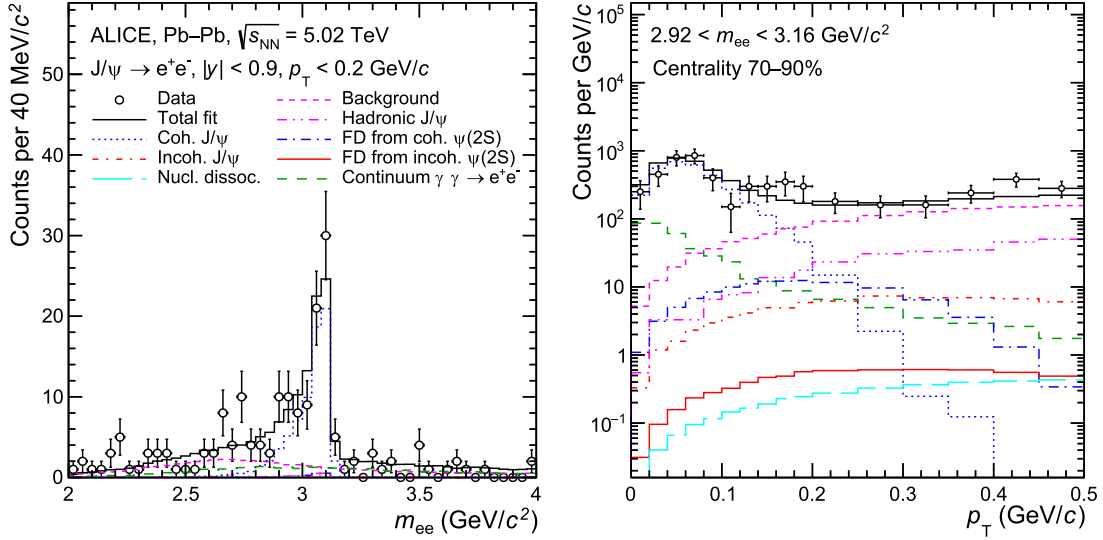


Fig. 1. Invariant mass distribution for $p_T < 200$ MeV/c (left panel) and p_T distribution for $2.92 < m_{ee} < 3.16$ GeV/c² (right panel) in the centrality class 70–90% for dielectrons with $|y| < 0.9$ in Pb–Pb collisions at $\sqrt{s_{NN}} = 5.02$ TeV. Measured distributions for J/ψ candidates are shown as black markers and the fit components are shown as coloured lines, as explained in the legend.

Table 2

Systematic uncertainties on the coherent J/ψ cross section for different centrality intervals. The systematic sources marked with a (*) are considered to be correlated over centrality. All the systematic uncertainty sources are considered fully correlated over p_T .

Centrality	40–50%	50–70%	70–90%
Tracking (cut variations)*	3.3%	3.3%	3.3%
Tracking (ITS-TPC matching)*	6.5%	6.5%	6.5%
Electron identification*	2.1%	3.8%	3.8%
Fit (correlated bkg)	4.1%	0.4%	0.2%
Fit (hadronic J/ψ)	0.6%	1.3%	1.1%
Fit (coherent J/ψ)	3.1%	0.7%	0.15%
Fit range	2.2%	1.0%	0.4%
Signal extraction method	18.5%	3.5%	1.3%
Luminosity*	2.5%	2.5%	2.5%
Centrality definition*	2%	2%	1%
Branching ratio*	0.5%	0.5%	0.5%
Total	21.1%	9.7%	8.9%

The doubly-differential cross section of the coherent J/ψ photoproduction, $d^2\sigma/dydp_T$, for a rapidity interval, Δy , and a p_T interval, Δp_T , is computed as:

$$\frac{d^2\sigma}{dydp_T} = \frac{N_{J/\psi,\text{coh}}}{(A \times \epsilon)_{J/\psi,\text{coh}} \times BR(J/\psi \rightarrow e^+e^-) \times \Delta y \times \Delta p_T \times \mathcal{L}}, \quad (3)$$

where $N_{J/\psi,\text{coh}}$ is the raw yield of coherently photoproduced J/ψ , $(A \times \epsilon)_{J/\psi,\text{coh}}$ is the average acceptance and efficiency factor for the kinematic window studied, and \mathcal{L} is the integrated luminosity for the analysed data sample as given in Section 2, all referring to the centrality class considered. The obtained computed cross sections correspond to the luminosity integrated in the given centrality interval. The $BR(J/\psi \rightarrow e^+e^-)$ is the branching ratio of the J/ψ decay into the dielectron channel [44].

The acceptance times efficiency correction is the product of the kinematic acceptance, the tracking and particle identification (PID) efficiency, and the fraction of the signal contained within the invariant mass counting window. With the exception of the PID efficiency, all these factors are obtained based on a MC simulation of coherently photoproduced, transversely polarised J/ψ generated using STARLight and embedded in Pb–Pb collisions generated using HIJING, as described above. The J/ψ PID efficiency is estimated using a data-driven method, similar to the one described in Refs. [35,37], based on a pure sample of

electrons using tagged photon conversions. The total acceptance times efficiency correction is about 10% on average, with a p_T dependence which for the contributing factors listed above is quite mild in the $p_T < 0.5$ GeV/c range relevant here. However, there is some p_T migration between generator and detector level due to the J/ψ p_T resolution being of the same order as the typical p_T of the coherent photoproduced J/ψ , and due to the radiative J/ψ decay. The impact of bin migration was checked by applying an unfolding procedure to the measured raw spectrum, as described later in this section, and the differences were found to be negligible.

The systematic uncertainties affecting the measured cross sections originate from uncertainties on the tracking and particle identification efficiencies, signal extraction, collision centrality, luminosity determination, and the branching ratio of the J/ψ into dielectrons. A summary of all the uncertainties is provided in Table 2. The tracking uncertainty consists of two contributions, one from the ITS-TPC matching and one due to the choice of the track quality criteria, as also detailed in Ref. [35]. The former is taken as the difference observed between MC simulations and data for the single-track ITS-TPC matching efficiency, propagated to J/ψ candidate dielectrons, and amounts to about 6.5%. The latter is estimated by repeating the analysis with variations of the track quality criteria and amounts to approximately 3.3%. The uncertainty on the PID efficiency is estimated by varying the pion and proton exclusion cuts, as described in Refs. [35,37], and resulted in an uncertainty of 2.1% for the 40–50% and 3.8% for the 50–90% centrality ranges. The uncertainty on the signal extraction includes contributions from the templates used in the fit model described in Eq. (1), fit ranges, and signal counting method. The F_{bkg} template was changed by removing the correlated background component and thus keeping only the combinatorial component estimated with event mixing. Adopting a rather conservative approach, the F_{hadr} component is constructed with and without the tuning of the input p_T shape on experimental data, and the associated systematic error is taken as $1/\sqrt{12}$ of the difference of the resulting cross sections, corresponding to the ratio of the standard deviation and the full spread of a uniform distribution. The corresponding uncertainties from the F_{bkg} and F_{hadr} variations range between 0.2–4.1% and 0.6–1.1%, respectively. The F_{phot} template corresponding to the coherent photoproduction process was varied from its shape expected for UPC, assuming that the $\langle p_T \rangle$ of the distribution is inversely proportional to the radius of the target nucleus spectator region, with the radius being determined for each centrality range as $R \sim A_{\text{spec}}^{1/3}$, with $A_{\text{spec}} = A_{\text{Pb}} - \langle N_{\text{part}} \rangle / 2$. Hence,

the template shapes were modified for each centrality interval by shifting each entry in the original STARLight-generated template from p_T to $r p_T$, with $r = (A_{\text{Pb}}/A_{\text{spec}})^{1/3}$, plus a Gaussian smearing term, centred at zero, to avoid binning effects. The J/ψ yields extracted with these modified templates deviated from the default between 0.15 and 3.1%, depending on centrality, with the deviation growing towards more central collisions as expected. Variations of the fit ranges in invariant mass and transverse momentum led to systematic uncertainties between 0.35 and 2.2%, depending on centrality. The default signal counting method, integrating the J/ψ coherent photoproduction template, was changed to counting the entries left after subtracting all the other fit components. The extracted yields changed by 18.5%, 3.5%, and 1.3% for the centrality ranges 40–50%, 50–70%, and 70–90%, respectively. The uncertainty on the integrated luminosity is 2.5% and is determined in the analysis of the van der Meer scan runs as described in Ref. [45]. The uncertainty on the centrality selection is determined by running the analysis with centrality ranges shifted by 1% in either direction to account for uncertainties on the anchor point used in the centrality definition [46]. The variations of the extracted yields are compatible with statistical fluctuations, but we conservatively assigned a systematic uncertainty of 1% for the most peripheral centrality range and 2% for the rest. For the (y, p_T) doubly-differential cross sections, the systematic uncertainties are considered to a large extent correlated over p_T and uniform (global) in the p_T range relevant for coherent J/ψ photoproduction. An exception is the uncertainty due to the fit procedure, which is also strongly correlated over p_T ; however, the size of the uncertainties have point-to-point variations and thus are not considered as global. The uncertainty on the $J/\psi \rightarrow e^+e^-$ branching ratio is quoted as 0.5% [44].

Two methodical cross checks were performed for the analysis. For the first one, the fixed weights $w_{\text{phot},i}$ adopted from Ref. [9] for the photoproduced components $F_{\text{phot},i}$, were grouped according to their origin: the weights for the coherent and incoherent charmonium production plus the $\gamma\gamma \rightarrow e^+e^-$ continuum were left free in the fit, while keeping the same ratio as in Ref. [9] between feed-down and direct production for the coherent and incoherent components. This approach gave very similar results to the default method, and no associated systematic error was assigned. The second cross check involved using an unfolding procedure instead of the acceptance times efficiency correction to obtain the doubly-differential cross sections, in order to quantify possible effects due to the J/ψ kinematic variation between the generator and detector level. The response matrix was constructed using the MC simulations for coherently photoproduced J/ψ , and the unfolding was performed using both the Bayes [47] and Single Value Decomposition [48] methods with different values for the regularisation parameter. The difference relative to the default method was found to be negligible in this case as well, and no systematic uncertainty was assigned.

4. Results

The left panel of Fig. 2 shows the coherent J/ψ photoproduction cross section $d\sigma/dy$, extracted at midrapidity ($|y| < 0.9$), as a function of $\langle N_{\text{part}} \rangle$, for the centrality classes 70–90%, 50–70%, and 40–50%. Systematic uncertainties (excluding the global contribution from the beam luminosity) are depicted as open boxes, while the global centrality-independent systematic uncertainty of 2.5% is quoted in the legend. The measured cross sections show a mild centrality dependence, within uncertainties compatible with no variation within the studied centrality range. It should be noted that, as pointed out in the Section 3, the cross sections are integrated in their respective centrality intervals and that the three data points cover different fractions of the total Pb–Pb cross section. Namely, the semicentral data point (40–50%) covers 10% while the two most peripheral data points each cover 20% of the total cross section. The experimental results are compared with a set of theoretical models, as indicated in the legend.

The calculations are based on the UPC description of vector meson photoproduction in terms of a convolution of the photon flux and the

photonuclear cross section, but integrating only over the impact parameter range corresponding to the centrality class of interest. The overlapping region in the collision, with hadronic interactions, is considered in some of the calculations by introducing modifications of the photon flux and/or the photonuclear cross section, depending on the model. The GG-hs model by Cepila et al. [19] includes no modifications relative to the UPC picture except the specification of the impact parameter interval. Attempting to describe both coherent and incoherent photoproduction, this model employs an energy-dependent representation of subnucleonic degrees of freedom. This is modelled in terms of hot spots and a colour-dipole proton cross section taking low- x saturation effects into account [49], and using the Glauber-Gribov formalism to extrapolate the calculation from nucleonic to nuclear targets. In the set of predictions by Gay-Ducati et al. [18] labelled GBW and IIM, an effective photon flux is defined by integrating over photons reaching the nuclear target and disregarding those hitting the overlap region. These calculations consider two scenarios, denoted in Fig. 2 as S2 and S3, with S2 modifying the photon flux only while S3 in addition restricts the photonuclear cross section, excluding contributions from the hadronically interacting overlap zone. The GBW [49] and the IIM [50] descriptions employ different treatments of saturation effects in the colour-dipole proton cross section, based on parameterisations of DIS data. The approach by Zha et al. [20,21] takes into account the potential effect on photon and gluon emission by the hadronically interacting overlapping zone, exploring different scenarios regarding the roles of participants and spectators. In addition, these calculations consider the implications of the destructive interference between the photon amplitudes from the two nuclear sources moving in opposite directions. The estimates from Ref. [21] shown in Fig. 2 include nuclear shadowing effects and assume an unaltered photon emission from the overlapping region except for interference effects, combined with the disruption of photoproduction in the participant region.

The experimental results are qualitatively well described by the model calculations, although for the two most peripheral intervals, the absolute values of the cross sections are overestimated by all models. In particular, the calculations by Gay-Ducati et al. [18] for scenario S3, which take into account suppression of photoproduction in the overlap zone, are the most compatible with the data with a statistical significance of the differences averaged over the three centrality intervals of less than 2σ . However, the S2 scenario from Ref. [18] overestimates the measured cross section for all studied centrality intervals and the statistical compatibility with the data is around 3σ . It is worth noting that a modification of the photonuclear cross section might not be the only mechanism that explains the data. ALICE measurements at forward rapidity [17], which are qualitatively similar in trend and model comparisons to the results at midrapidity, are well described by the calculations by Klusek-Gawenda [22], which only assume inhibition of the photon flux in the overlap region.

The comparison with data at forward rapidity might also provide information on any final-state QGP influence on photoproduced charmonia. Such effects are naively expected to be more pronounced at midrapidity, where a higher medium temperature and energy density are expected [51]. The J/ψ photoproduction at mid- and forward rapidity are compared after normalising the measurements to the coherent J/ψ photoproduction cross section measured in UPC in the same rapidity interval in order to compensate for the rapidity dependence of photon flux and photo-nuclear cross section. Uncertainties which are correlated between the results in collisions with overlap and those in UPC are cancelled in the ratio. There are also two small differences in the kinematic coverage of the UPC results compared to those from peripheral or semicentral collisions. Namely, the midrapidity UPC coherent J/ψ yield is measured at $|y| < 0.8$ and the p_T range for the forward-rapidity one is $p_T < 0.25$ GeV/ c . This ratio ($\sigma_{\text{PC}}/\sigma_{\text{UPC}}$), corrected for the different centrality interval widths ΔC , is shown in the right panel of Fig. 2 as a function of $\langle N_{\text{part}} \rangle$, for forward ($2.5 < y < 4$) and midrapidity ($|y| < 0.9$). The measurements at forward rapidity in peripheral collisions are

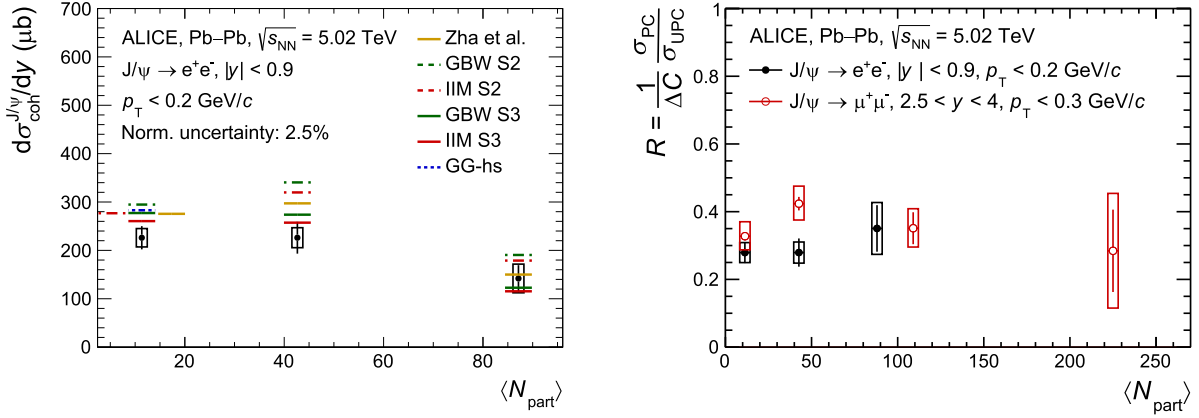


Fig. 2. Left: Coherent J/ψ cross section as a function of $\langle N_{\text{part}} \rangle$ in Pb–Pb collisions at $\sqrt{s_{\text{NN}}} = 5.02$ TeV at midrapidity. The statistical uncertainties are shown as bars, while the systematic uncertainties (excluding the global contribution from the beam luminosity) are shown as boxes. It should be noted that the interval 40–50% is half as wide as the two more peripheral ones, 50–70% and 70–90%. Data are compared to calculations from W. Zha et al. [20,21], Gay-Ducati et al. (GBW S2/S3 and IIM S2/S3) [18], and Cepila et al. (GG-hs) [19]. For the interval 70–90%, the calculations from W. Zha et al. and IIM S2 are shifted on the x-axis for visibility. Right: Coherent J/ψ cross section as a function of $\langle N_{\text{part}} \rangle$ measured at midrapidity (black markers) and forward rapidity (red markers) [17] normalised to the corresponding cross sections measured in the same rapidity ranges in UPC [8,9] and corrected for the centrality interval width ΔC .

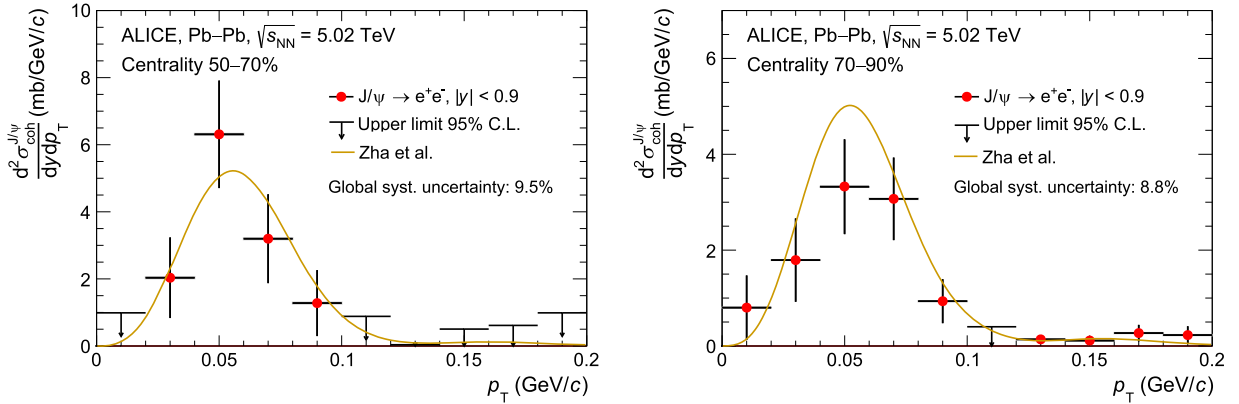


Fig. 3. Coherent J/ψ cross section as a function of p_T in Pb–Pb collisions at $\sqrt{s_{\text{NN}}} = 5.02$ TeV measured in the 50–70% and 70–90% centrality classes. The error bars indicate statistical uncertainties, while the systematic uncertainties, excluding those considered as global (see text for details), are shown as boxes. Data are compared to calculations from W. Zha et al. [20,21].

taken from Ref. [17], while the UPC results for the two rapidity intervals are from Refs. [8,9]. Within uncertainties, the ratios at the two rapidities are statistically compatible over the common centrality range, and show a nearly flat evolution with $\langle N_{\text{part}} \rangle$. Notably, the measurements for the most peripheral collisions, 70–90%, which are also the most precise, are in very good agreement. The measured cross sections in this analysis show no hints of QGP effects, but the centrality range studied is rather limited, extending only up to $\langle N_{\text{part}} \rangle < 100$, which, combined with the large experimental uncertainties, may be insufficient to reveal any medium-induced suppression. Additional rapidity dependent effects on the photon flux due to the nuclear overlap may complicate this naive phenomenological picture, hence further model calculations are required for a deeper insight. The large increase in luminosity to be collected during the LHC Run 3 and 4 is expected to extend the range of the J/ψ measurement up to the most central collisions and also give access to the centrality dependent photoproduction of the less bound $\psi(2S)$, important for shedding light on these phenomenological aspects.

Fig. 3 shows the doubly-differential cross section $d^2\sigma/dydp_T$ for the rapidity interval $|y| < 0.9$ and in the centrality classes 50–70% (left) and 70–90% (right), which was obtained by subtracting from the measured distribution $N(m_{ee}, p_T)$ all of the fitted templates with the exception of the one corresponding to the coherently photoproduced J/ψ . The p_T -independent systematic uncertainties are quoted in the legend for the two centralities as global uncertainties, while the point-to-point system-

atic uncertainties related to the fit of the two-dimensional (m_{ee}, p_T) pair distributions are shown as boxes around the data points and are very small compared to the global ones and the statistical uncertainties. The theoretical calculations by Zha et al., described above [20,21], in which the nucleons in the overlapping zone do not participate in the photoproduction, are in good agreement with ALICE measurements within the large experimental uncertainties. This model was also found to reproduce the shape of the LHCb p_T differential measurements, but appears to underpredict the reported yield [16]. In the model, the rapid decline of the cross section towards $p_T = 0$ is ascribed to the destructive interference between photon amplitudes from the two collision partners, while the bulk of the distribution and the tail towards higher p_T carry information about the target size and spatial distribution. In particular, a variation of the p_T differential cross section is expected with centrality. The observed shapes of the p_T spectra in the 50–70% and 70–90% centrality classes are compatible with the current experimental uncertainties, however, only a very weak centrality dependence is predicted in this centrality range, as seen from the theory calculation shown in Fig. 3.

5. Conclusions

In summary, this paper reports on the measurement of coherent J/ψ photoproduction cross section as a function of p_T and

collision centrality, for peripheral and semicentral Pb – Pb collisions at $\sqrt{s_{NN}} = 5.02$ TeV., for the first time at midrapidity ($|y| < 0.9$) at LHC energies. The reported observations extend and complement earlier measurements published by ALICE and LHCb at forward rapidity, and STAR at midrapidity at a lower collision energy. The p_T -integrated cross section exhibits a mild centrality dependence compatible with no variation over the centrality interval studied and is qualitatively similar to the corresponding observations at forward rapidity. Within the large uncertainties, the centrality-dependent measurements are fairly well described by several sets of theoretical calculations, based on the UPC description of vector meson photoproduction and modified to take into account the nuclear overlap in the collisions, but not incorporating effects from a hot expanding QGP. The combined ALICE measurements at mid- and forward rapidity favour models with inhibition of photon flux only, or inhibition of the photon flux together with a suppression of charmonium generation in the hadronic overlap region. Within uncertainties, the measured cross sections show no suppression beyond the present model predictions. The p_T -integrated cross sections measured at mid- and forward rapidity by ALICE, normalised to the cross sections measured in the same rapidity ranges in UPC [8,9], are in good agreement within uncertainties. The p_T -differential cross sections are well described by calculations taking into account the interference between the two photon emitters as well as the effect of strong interactions in the overlap zone. Future data-taking campaigns during the LHC Run 3 and Run 4 [52], with a foreseen increase in statistics of a factor of about 100 at midrapidity, are expected to facilitate photoproduction measurements for central collisions (0–10%) and precision measurements of p_T -differential cross sections for non-central collisions (above 10%). This will help elucidate the influence of the nuclear overlap region on the coherent J/ψ photoproduction, including possible final-state effects from the expanding QGP.

Data availability

This manuscript has associated data in a HEPData repository at: <https://www.hepdata.net/record/ins2829848>.

Declaration of competing interest

The authors declare that they have no known competing financial interests or personal relationships that could have appeared to influence the work reported in this paper.







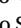

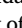





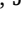

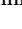

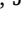

Acknowledgements

The ALICE Collaboration would like to thank all its engineers and technicians for their invaluable contributions to the construction of the experiment and the CERN accelerator teams for the outstanding performance of the LHC complex. The ALICE Collaboration gratefully acknowledges the resources and support provided by all Grid centres and the Worldwide LHC Computing Grid (WLCG) collaboration. The ALICE Collaboration acknowledges the following funding agencies for their support in building and running the ALICE detector: A. I. Alikhanyan National Science Laboratory (Yerevan Physics Institute) Foundation (ANSL), State Committee of Science and World Federation of Scientists (WFS), Armenia; Austrian Academy of Sciences, Austrian Science Fund (FWF): [M 2467-N36] and Nationalstiftung für Forschung, Technologie und Entwicklung, Austria; Ministry of Communications and High Technologies, National Nuclear Research Center, Azerbaijan; Conselho Nacional de Desenvolvimento Científico e Tecnológico (CNPq), Financiadora de Estudos e Projetos (Finep), Fundação de Amparo à Pesquisa do Estado de São Paulo (FAPESP) and Universidade Federal do Rio Grande do Sul (UFRGS), Brazil; Bulgarian Ministry of Education and Science, within the National Roadmap for Research Infrastructures 2020–2027 (object CERN), Bulgaria; Ministry of Education of China (MOEC),

Ministry of Science & Technology of China (MSTC) and National Natural Science Foundation of China (NSFC), China; Ministry of Science and Education and Croatian Science Foundation, Croatia; Centro de Aplicaciones Tecnológicas y Desarrollo Nuclear (CEADEN), Cubaenergía, Cuba; Ministry of Education, Youth and Sports of the Czech Republic, Czech Republic; The Danish Council for Independent Research | Natural Sciences, the VILLUM FONDEN and Danish National Research Foundation (DNRF), Denmark; Helsinki Institute of Physics (HIP), Finland; Commissariat à l’Energie Atomique (CEA) and Institut National de Physique Nucléaire et de Physique des Particules (IN2P3) and Centre National de la Recherche Scientifique (CNRS), France; Bundesministerium für Bildung und Forschung (BMBF) and GSI Helmholtzzentrum für Schwerionenforschung GmbH, Germany; General Secretariat for Research and Technology, Ministry of Education, Research and Religions, Greece; National Research, Development and Innovation Office, Hungary; Department of Atomic Energy Government of India (DAE), Department of Science and Technology, Government of India (DST), University Grants Commission, Government of India (UGC) and Council of Scientific and Industrial Research (CSIR), India; National Research and Innovation Agency - BRIN, Indonesia; Istituto Nazionale di Fisica Nucleare (INFN), Italy; Japanese Ministry of Education, Culture, Sports, Science and Technology (MEXT) and Japan Society for the Promotion of Science (JSPS) KAKENHI, Japan; Consejo Nacional de Ciencia (CONACYT) y Tecnología, through Fondo de Cooperación Internacional en Ciencia y Tecnología (FONCICYT) and Dirección General de Asuntos del Personal Académico (DGAPA), Mexico; Nederlandse Organisatie voor Wetenschappelijk Onderzoek (NWO), Netherlands; The Research Council of Norway, Norway; Pontificia Universidad Católica del Perú, Peru; Ministry of Science and Higher Education, National Science Centre and WUT ID-UB, Poland; Korea Institute of Science and Technology Information and National Research Foundation of Korea (NRF), Republic of Korea; Ministry of Education and Scientific Research, Institute of Atomic Physics, Ministry of Research and Innovation and Institute of Atomic Physics and Universitatea Nationala de Stiinta si Tehnologie Politehnica Bucuresti, Romania; Ministry of Education, Science, Research and Sport of the Slovak Republic, Slovakia; National Research Foundation of South Africa, South Africa; Swedish Research Council (VR) and Knut & Alice Wallenberg Foundation (KAW), Sweden; European Organization for Nuclear Research, Switzerland; Suranaree University of Technology (SUT), National Science and Technology Development Agency (NSTDA) and National Science, Research and Innovation Fund (NSRF via PMU-B B05F650021), Thailand; Turkish Energy, Nuclear and Mineral Research Agency (TENMAK), Turkey; National Academy of Sciences of Ukraine, Ukraine; Science and Technology Facilities Council (STFC), United Kingdom; National Science Foundation of the United States of America (NSF) and United States Department of Energy, Office of Nuclear Physics (DOE NP), United States of America. In addition, individual groups or members have received support from: Czech Science Foundation (grant no. 23-07499S), Czech Republic; FORTE project, reg. no. CZ.02.01.01/00/22_008/0004632, Czech Republic, co-funded by the European Union, Czech Republic; [European Research Council](#) (grant no. 950692), European Union; ICSC - Centro Nazionale di Ricerca in High Performance Computing, Big Data and Quantum Computing, European Union - NextGenerationEU; [Academy of Finland](#) (Center of Excellence in Quark Matter) (grant nos. 346327, 346328), Finland.

Appendix

The ALICE Collaboration

S. Acharya ¹²⁷, A. Agarwal¹³⁵, G. Aglieri Rinella ³², L. Aglietta ²⁴, M. Agnello ²⁹, N. Agrawal ²⁵, Z. Ahammed ¹³⁵, S. Ahmad ¹⁵, S.U. Ahn ⁷¹, I. Ajuja ³⁷, A. Akintinov ¹⁴⁰, V. Akishina³⁸, M. Al-Turany ⁹⁷, D. Aleksandrov ¹⁴⁰, B. Alessandro ⁵⁶, H.M. Alfanda ⁶, R. Alfaro Molina ⁵⁷, B. Ali ¹⁵, A. Alici ²⁵, N. Alizadehvandchali ¹¹⁶, A. Alkin ¹⁰⁴, J. Alme ²⁰,

G. Alocco ^{24,52}, T. Alt ⁶⁴, A.R. Altamura ⁵⁰, I. Altsybeev ⁹⁵, J.R. Alvarado ⁴⁴, C.O.R. Alvarez ⁴⁴, M.N. Anaam ⁶, C. Andrei ⁴⁵, N. Andreou ¹¹⁵, A. Andronic ¹²⁶, E. Andronov ¹⁴⁰, V. Anguelov ⁹⁴, F. Antinori ⁵⁴, P. Antonioli ⁵¹, N. Apadula ⁷⁴, L. Aphecetche ¹⁰³, H. Appelhäuser ⁶⁴, C. Arata ⁷³, S. Arcelli ²⁵, R. Arnaldi ⁵⁶, J.G.M.C.A. Arneiro ¹¹⁰, I.C. Arsene ¹⁹, M. Arslanodk ¹³⁸, A. Augustinus ³², R. Averbek ⁹⁷, D. Averyanov ¹⁴⁰, M.D. Azmi ¹⁵, H. Baba ¹²⁴, A. Badalà ⁵³, J. Bae ¹⁰⁴, Y.W. Baek ⁴⁰, X. Bai ¹²⁰, R. Bailhache ⁶⁴, Y. Bailung ⁴⁸, R. Bala ⁹¹, A. Balbino ²⁹, A. Baldisseri ¹³⁰, B. Balis ², Z. Banoo ⁹¹, V. Barbasova ³⁷, F. Barile ³¹, L. Barioglio ⁵⁶, M. Barlou ⁷⁸, B. Barman ⁴¹, G.G. Barnaföldi ⁴⁶, L.S. Barnby ¹¹⁵, E. Barreau ¹⁰³, V. Barret ¹²⁷, L. Barreto ¹¹⁰, C. Bartels ¹¹⁹, K. Barth ³², E. Bartsch ⁶⁴, N. Bastid ¹²⁷, S. Basu ^{75,1}, G. Batigne ¹⁰³, D. Battistini ⁹⁵, B. Batyunya ¹⁴¹, D. Bauri ⁴⁷, J.L. Bazo Alba ¹⁰¹, I.G. Bearden ⁸³, C. Beattie ¹³⁸, P. Becht ⁹⁷, D. Behera ⁴⁸, I. Belikov ¹²⁹, A.D.C. Bell Hechavarría ¹²⁶, F. Bellini ²⁵, R. Bellwied ¹¹⁶, S. Belokurova ¹⁴⁰, L.G.E. Beltran ¹⁰⁹, Y.A.V. Beltran ⁴⁴, G. Bencedi ⁴⁶, A. Bensaoula ¹¹⁶, S. Beole ²⁴, Y. Berdnikov ¹⁴⁰, A. Berdnikova ⁹⁴, L. Bergmann ⁹⁴, M.G. Besoiu ⁶³, L. Betev ³², P.P. Bhaduri ¹³⁵, A. Bhasin ⁹¹, B. Bhattacharjee ⁴¹, L. Bianchi ²⁴, J. Bielčik ³⁵, J. Bielčiková ⁸⁶, A.P. Bigot ¹²⁹, A. Bilandzic ⁹⁵, G. Biro ⁴⁶, S. Biswas ⁴, N. Bize ¹⁰³, J.T. Blair ¹⁰⁸, D. Blau ¹⁴⁰, M.B. Blidaru ⁹⁷, N. Bluhme ³⁸, C. Blume ⁶⁴, G. Boca ^{21,55}, F. Bock ⁸⁷, T. Bodova ²⁰, J. Bok ¹⁶, L. Boldizsár ⁴⁶, M. Bombara ³⁷, P.M. Bond ³², G. Bonomi ^{134,55}, H. Borel ¹³⁰, A. Borissov ¹⁴⁰, A.G. Borquez Carcamo ⁹⁴, E. Botta ²⁴, Y.E.M. Bouziani ⁶⁴, L. Bratrud ⁶⁴, P. Braun-Munzinger ⁹⁷, M. Bregant ¹¹⁰, M. Broz ³⁵, G.E. Bruno ^{96,31}, V.D. Buchachiev ³⁶, M.D. Buckland ⁸⁵, D. Budnikov ¹⁴⁰, H. Buesching ⁶⁴, S. Bufalino ²⁹, P. Buhler ¹⁰², N. Burmasov ¹⁴⁰, Z. Buthelezi ^{68,123}, A. Bylinkin ²⁰, S.A. Bysiack ¹⁰⁷, J.C. Cabanillas Noris ¹⁰⁹, M.F.T. Cabrera ¹¹⁶, M. Cai ⁶, H. Caines ¹³⁸, A. Caliva ²⁸, E. Calvo Villar ¹⁰¹, J.M.M. Camacho ¹⁰⁹, P. Camerini ²³, F.D.M. Canedo ¹¹⁰, S.L. Cantway ¹³⁸, M. Carabas ¹¹³, A.A. Carballo ³², F. Carnesecchi ³², R. Caron ¹²⁸, L.A.D. Carvalho ¹¹⁰, J. Castillo Castellanos ¹³⁰, M. Castoldi ³², F. Catalano ³², S. Cattaruzzi ²³, C. Ceballos Sanchez ⁷, R. Cerri ²⁴, I. Chakaberia ⁷⁴, P. Chakraborty ¹³⁶, S. Chandra ¹³⁵, S. Chapeland ³², M. Chartier ¹¹⁹, S. Chattopadhyay ¹³⁵, S. Chattopadhyay ¹³⁵, S. Chattopadhyay ⁹⁹, M. Chen ³⁹, T. Cheng ⁶, C. Cheshkov ¹²⁸, V. Chibante Barroso ³², D.D. Chinellato ¹⁰², E.S. Chizzali ^{11,95}, J. Cho ⁵⁸, S. Cho ⁵⁸, P. Chochula ³², Z.A. Chochulska ¹³⁶, D. Choudhury ⁴¹, P. Christakoglou ⁸⁴, C.H. Christensen ⁸³, P. Christiansen ⁷⁵, T. Chujo ¹²⁵, M. Ciaccio ²⁹, C. Cicalo ⁵², M.R. Ciupek ⁹⁷, G. Clai ^{111,51}, F. Colamaria ⁵⁰, J.S. Colburn ¹⁰⁰, D. Colella ³¹, A. Colelli ³¹, M. Colocci ²⁵, M. Concas ³², G. Conesa Balbastre ⁷³, Z. Conesa del Valle ¹³¹, G. Contino ²³, J.G. Contreras ³⁵, M.L. Coquet ¹⁰³, P. Cortese ^{133,56}, M.R. Cosentino ¹¹², F. Costa ³², S. Costanza ^{21,55}, C. Cot ¹³¹, P. Crochet ¹²⁷, R. Cruz-Torres ⁷⁴, M.M. Czarnynoga ¹³⁶, A. Dainese ⁵⁴, G. Dange ³⁸, M.C. Danisch ⁹⁴, A. Danu ⁶³, P. Das ⁸⁰, S. Das ⁴, A.R. Dash ¹²⁶, S. Dash ⁴⁷, A. De Caro ²⁸, G. de Cataldo ⁵⁰, J. de Coveland ³⁸, A. De Falco ²², D. De Gruttola ²⁸, N. De Marco ⁵⁶, C. De Martin ²³, S. De Pasquale ²⁸, R. Deb ¹³⁴, R. Del Grande ⁹⁵, L. Dello Stritto ³², W. Deng ⁶, K.C. Devereaux ¹⁸, P. Dhankeher ¹⁸, D. Di Bari ³¹, A. Di Mauro ³², B. Di Ruzza ¹³², B. Diab ¹³⁰, R.A. Diaz ^{141,7}, T. Dietel ¹¹⁴, Y. Ding ⁶, J. Ditzel ⁶⁴, R. Divià ³², Ø. Djuvsland ²⁰, U. Dmitrieva ¹⁴⁰, A. Dobrin ⁶³, B. Dönigus ⁶⁴, J.M. Dubinski ¹³⁶, A. Dubla ⁹⁷, P. Dupieux ¹²⁷, N. Dzalaliova ¹³, T.M. Eder ¹²⁶, R.J. Ehlers ⁷⁴, F. Eisenhut ⁶⁴, R. Ejima ⁹², D. Elia ⁵⁰, B. Erasmus ¹⁰³, F. Ercolessi ²⁵, B. Espagnon ¹³¹, G. Eulisse ³², D. Evans ¹⁰⁰, S. Evdokimov ¹⁴⁰, L. Fabbietti ⁹⁵, M. Faggin ²³, J. Favre ⁷³, F. Fan ⁶, W. Fan ⁷⁴, A. Fantoni ⁴⁹, M. Fasel ⁸⁷, A. Feliciello ⁵⁶, G. Feofilov ¹⁴⁰, A. Fernández Téllez ⁴⁴, L. Ferrandi ¹¹⁰, M.B. Ferrer ³², A. Ferrero ¹³⁰, C. Ferrero ^{14,56}, A. Ferretti ²⁴, V.J.G. Feuillard ⁹⁴, V. Filova ³⁵, D. Finogeev ¹⁴⁰, F.M. Fionda ⁵², E. Flatland ³², F. Flor ^{138,116}, A.N. Flores ¹⁰⁸, S. Foertsch ⁶⁸, I. Fokin ⁹⁴, S. Fokin ¹⁴⁰, U. Follo ^{14,56}, E. Fragiaco ⁵⁷, E. Frajna ⁴⁶, U. Fuchs ³², N. Funicello ²⁸, C. Furget ⁷³, A. Furs ¹⁴⁰, T. Fusayasu ⁹⁸, J.J. Gaardhøje ⁸³, M. Gagliardi ²⁴, A.M. Gago ¹⁰¹, T. Gahlaut ⁴⁷, C.D. Galvan ¹⁰⁹, S. Gami ⁸⁰, D.R. Gangadharan ¹¹⁶, P. Ganoti ⁷⁸, C. Garabatos ⁹⁷, J.M. Garcia ⁴⁴, T. García Chávez ⁴⁴, E. Garcia-Solis ⁹, C. Gargiulo ³², P. Gasik ⁹⁷, H.M. Gaur ³⁸, A. Gautam ¹¹⁸, M.B. Gay Ducati ⁶⁶, M. Germain ¹⁰³, R.A. Gernhaeuser ⁹⁵, C. Ghosh ¹³⁵, M. Giacalone ⁵¹, G. Gioachin ²⁹, S.K. Giri ¹³⁵, P. Giubellino ^{97,56}, P. Giubilato ²⁷, A.M.C. Glaenger ¹³⁰, P. Gläsel ⁹⁴, E. Glimos ¹²², D.J.Q. Goh ⁷⁶, V. Gonzalez ¹³⁷, P. Gordeev ¹⁴⁰, M. Gorgon ², K. Goswami ⁴⁸, S. Gotovac ³³, V. Grabski ⁶⁷, L.K. Graczykowski ¹³⁶, E. Grecka ⁸⁶, A. Grelli ⁵⁹, C. Grigoras ³², V. Grigoriev ¹⁴⁰, S. Grigoryan ^{141,1}, F. Grosa ³², J.F. Grosse-Oetringhaus ³², R. Grosso ⁹⁷, D. Grund ³⁵, N.A. Grunwald ⁹⁴, G.G. Guardiano ¹¹¹, R. Guernane ⁷³, M. Guimbaud ¹⁰³, K. Gulbrandsen ⁸³, J.J.W.K. Gumprecht ¹⁰², T. Gündem ⁶⁴, T. Gunji ¹²⁴, W. Guo ⁶, A. Gupta ⁹¹, R. Gupta ⁹¹, R. Gupta ⁴⁸, K. Gwizdz ¹³⁶, L. Gyulai ⁴⁶, C. Hadjidakis ¹³¹, F.U. Haider ⁹¹, S. Haidlova ³⁵, M. Haldar ⁴, H. Hamagaki ⁷⁶, Y. Han ¹³⁹, B.G. Hanley ¹³⁷, R. Hannigan ¹⁰⁸, J. Hansen ⁷⁵, M.R. Haque ⁹⁷, J.W. Harris ¹³⁸, A. Harton ¹⁰⁹, M.V. Hartung ⁶⁴, H. Hassan ¹¹⁷, D. Hatzifotiadiou ⁵¹, P. Hauer ⁴², L.B. Havener ¹³⁸, E. Hellbär ³², H. Helstrup ³⁴, M. Hemmer ⁶⁴, T. Herman ³⁵, S.G. Hernandez ¹¹⁶, G. Herrera Corral ⁸, S. Herrmann ¹²⁸, K.F. Hetland ³⁴, B. Heybeck ⁶⁴, H. Hillemanns ³², B. Hippolyte ¹²⁹, I.P.M. Hobus ⁸⁴, F.W. Hoffmann ⁷⁰, B. Hofman ⁵⁹, G.H. Hong ¹³⁹, M. Horst ⁹⁵, A. Horzyk ², Y. Hou ⁶, P. Hristov ³², P. Huhn ⁶⁴, L.M. Huhta ¹¹⁷, T.J. Humanic ⁸⁸, A. Hutson ¹¹⁶, D. Hutter ³⁸, M.C. Hwang ¹⁸, R. Ilkaev ¹⁴⁰, M. Inaba ¹²⁵, G.M. Innocenti ³², M. Ippolitov ¹⁴⁰, A. Isakov ⁸⁴, T. Isidori ¹¹⁸, M.S. Islam ⁹⁹, S. Iurchenko ¹⁴⁰, M. Ivanov ¹³, M. Ivanov ⁹⁷, V. Ivanov ¹⁴⁰, K.E. Iversen ⁷⁵, M. Jablonski ², B. Jacak ^{18,74}, N. Jacazio ²⁵, P.M. Jacobs ⁷⁴, S. Jadlovská ¹⁰⁶, J. Jadlovsky ¹⁰⁶, S. Jaelani ⁸², C. Jahnke ¹¹⁰, M.J. Jakubowska ¹³⁶, M.A. Janik ¹³⁶, T. Janson ⁷⁰, S. Ji ¹⁶, S. Jia ¹⁰, T. Jiang ¹⁰, A.A.P. Jimenez ⁶⁵, F. Jonas ⁷⁴, D.M. Jones ¹¹⁹, J.M. Jowett ^{32,97}, J. Jung ⁶⁴, M. Jung ⁶⁴, A. Junique ³², A. Jusko ¹⁰⁰, J. Kaewjai ¹⁰⁵, P. Kalinak ⁶⁰, A. Kalweit ³², A. Karasu Uysal ^{10,72}, D. Karatovic ⁸⁹, N. Karatzenis ¹⁰⁰, O. Karavichev ¹⁴⁰, T. Karavicheva ¹⁴⁰, E. Karpechev ¹⁴⁰, M.J. Karwowska ^{32,136}, U. Keschull ⁷⁰, M. Keil ³², B. Ketzer ⁴², J. Keul ⁶⁴, S.S. Khade ⁴⁸, A.M. Khan ¹²⁰, S. Khan ¹⁵, A. Khanzadeev ¹⁴⁰, Y. Kharlov ¹⁴⁰, A. Khatun ¹¹⁸, A. Khuntia ³⁵, Z. Khuramova ⁶⁴, B. Kileng ³⁴, B. Kim ¹⁰⁴, C. Kim ¹⁶, D.J. Kim ¹¹⁷, E.J. Kim ⁶⁹, J. Kim ¹³⁹, J. Kim ⁵⁸, J. Kim ^{32,69}, M. Kim ¹⁸, S. Kim ¹⁷, T. Kim ¹³⁹, K. Kimura ⁹², A. Kirkova ³⁶, S. Kirsch ⁶⁴, I. Kisel ³⁸, S. Kiselev ¹⁴⁰, A. Kisiel ¹³⁶, J.P. Kitowski ², J.L. Klay ⁵, J. Klein ³², S. Klein ⁷⁴, C. Klein-Bösing ¹²⁶, M. Kleiner ⁶⁴, T. Klemenz ⁹⁵, A. Kluge ³², C. Kobdaj ¹⁰⁵, R. Kohara ¹²⁴, T. Kollegger ⁹⁷, A. Kondratyev ¹⁴¹, N. Kondratyeva ¹⁴⁰, J. König ⁶⁴, S.A. Königstorfer ⁹⁵, P.J. Konopka ³², G. Kornakov ¹³⁶, M. Korwieser ⁹⁵, S.D. Koryciak ², C. Koster ⁸⁴, A. Kotliarov ⁸⁶, N. Kovacic ⁸⁹, V. Kovalenko ¹⁴⁰, M. Kowalski ¹⁰⁷, V. Kozuharov ³⁶, G. Kozlov ³⁸, I. Králik ⁶⁰, A. Kravčáková ³⁷, L. Krcal ^{32,38}, M. Krivda ^{100,60}, F. Krizek ⁸⁶, K. Krizkova Gajdosova ³², C. Krug ⁶⁶, M. Krüger ⁶⁴, D.M. Krupova ³⁵, E. Kryshen ¹⁴⁰, V. Kučera ⁵⁸, C. Kuhn ¹²⁹, P.G. Kuijter ^{84,1}, T. Kumaoka ¹²⁵, D. Kumar ¹³⁵, L. Kumar ⁹⁰, N. Kumar ⁹⁰, S. Kumar ¹⁰, S. Kundu ³², P. Kurashvili ⁷⁹, A. Kurepin ¹⁴⁰, A.B. Kurepin ¹⁴⁰, A. Kuryakin ¹⁴⁰, S. Kuschpil ⁸⁶, V. Kuskov ¹⁴⁰, M. Kutyla ¹³⁶, A. Kuznetsov ¹⁴¹, M.J. Kweon ⁵⁸, Y. Kwon ¹³⁹, S.L. La

Pointe ³⁸, P. La Rocca ²⁶, A. Lakrathok ¹⁰⁵, M. Lamanna ³², A.R. Landou ⁷³, R. Langoy ¹²¹, P. Lariou ³², E. Laudi ³², L. Lautner ^{32,95}, R.A.N. Laveaga ¹⁰⁹, R. Lavicka ¹⁰², R. Lea ^{134,55}, H. Lee ¹⁰⁴, I. Legrand ⁴⁵, G. Le gras ¹²⁶, J. Lehrbach ³⁸, A.M. Lejeune ³⁵, T.M. Lelek ², R.C. Lemmon ^{1,85}, I. León Monzón ¹⁰⁹, M.M. Lesch ⁹⁵, E.D. Lesser ¹⁸, P. Lévai ⁴⁶, M. Li ⁶, P. Li ¹⁰, X. Li ¹⁰, B.E. Liang-Gilman ¹⁸, J. Lien ¹²¹, R. Lietava ¹⁰⁰, I. Likmeta ¹¹⁶, B. Lim ²⁴, S.H. Lim ¹⁶, V. Lindenstruth ³⁸, C. Lippmann ⁹⁷, D.H. Liu ⁶, J. Liu ¹¹⁹, G.S.S. Liveraro ¹¹¹, I.M. Lofnes ²⁰, C. Loizides ⁸⁷, S. Lokos ¹⁰⁷, J. Lömker ⁵⁹, X. Lopez ¹²⁷, E. López Torres ⁷, C. Lotteau ¹²⁸, P. Lu ^{97,120}, Z. Lu ¹⁰, F.V. Lugo ⁶⁷, J.R. Luhder ¹²⁶, M. Lunardon ²⁷, G. Luparello ⁵⁷, Y.G. Ma ³⁹, M. Mager ³², A. Maire ¹²⁹, E.M. Majerz ², M.V. Makariev ³⁶, M. Malaev ¹⁴⁰, G. Malfattore ²⁵, N.M. Malik ⁹¹, S.K. Malik ⁹¹, L. Malinina ^{1, VIII, 141}, D. Mallick ¹³¹, N. Mallick ⁴⁸, G. Mandaglio ^{30,53}, S.K. Mandal ⁷⁹, A. Manea ⁶³, V. Manko ¹⁴⁰, F. Manso ¹²⁷, V. Manzari ⁵⁰, Y. Mao ⁶, R.W. Marcjan ², G.V. Margagliotti ²³, A. Margotti ⁵¹, A. Marín ⁹⁷, C. Markert ¹⁰⁸, C.F.B. Marquez ³¹, P. Martinengo ³², M.I. Martínez ⁴⁴, G. Martínez García ¹⁰³, M.P.P. Martins ¹¹⁰, S. Masciocchi ⁹⁷, M. Maserà ²⁴, A. Masoni ⁵², L. Massacrier ¹³¹, O. Massen ⁵⁹, A. Mastroserio ^{132,50}, O. Matonoha ⁷⁵, S. Mattiazzo ²⁷, A. Matyja ¹⁰⁷, F. Mazzaschi ^{32,24}, M. Mazzeilli ¹¹⁶, Y. Melikyan ⁴³, M. Melo ¹¹⁰, A. Menchaca-Rocha ⁶⁷, J.E.M. Mendez ⁶⁵, E. Meninno ¹⁰², A.S. Menon ¹¹⁶, M.W. Menzel ^{32,94}, M. Meres ¹³, Y. Miake ¹²⁵, L. Micheletti ³², D. Mihai ¹¹³, D.L. Mihaylov ⁹⁵, K. Mikhaylov ^{141,140}, N. Minafra ¹¹⁸, D. Miśkowiec ⁹⁷, A. Modak ¹³⁴, B. Mohanty ⁸⁰, M. Mohisin Khan ^{VI,15}, M.A. Molander ⁴³, S. Monira ¹³⁶, C. Mordasini ¹¹⁷, D.A. Moreira De Godoy ¹²⁶, I. Morozov ¹⁴⁰, A. Morsch ³², T. Mrnjavac ³², V. Muccifora ⁴⁹, S. Muhuri ¹³⁵, J.D. Mulligan ⁷⁴, A. Mulliri ²², M.G. Munhoz ¹¹⁰, R.H. Munzer ⁶⁴, H. Murakami ¹²⁴, S. Murray ¹¹⁴, L. Musa ³², J. Musinsky ⁶⁰, J.W. Myrcha ¹³⁶, B. Naik ¹²³, A.I. Nambrath ¹⁸, B.K. Nandi ⁴⁷, R. Nania ⁵¹, E. Nappi ⁵⁰, A.F. Nassirpour ¹⁷, V. Nastase ¹¹³, A. Nath ⁹⁴, S. Nath ¹³⁵, C. Nattrass ¹²², M.N. Naidenov ³⁶, A. Neagu ¹⁹, A. Negru ¹¹³, E. Nekrasova ¹⁴⁰, L. Nellen ⁶⁵, R. Nepeivoda ⁷⁵, S. Nese ¹⁹, N. Nicassio ⁵⁰, B.S. Nielsen ⁸³, E.G. Nielsen ⁸³, S. Nikolaev ¹⁴⁰, S. Nikulin ¹⁴⁰, V. Nikulin ¹⁴⁰, F. Noferini ⁵¹, S. Noh ¹², P. Nomokonov ¹⁴¹, J. Norman ¹¹⁹, N. Novitzky ⁸⁷, P. Nowakowski ¹³⁶, A. Nyanin ¹⁴⁰, J. Nystrand ²⁰, S. Oh ¹⁷, A. Ohlson ⁷⁵, V.A. Okorokov ¹⁴⁰, J. Oleniacz ¹³⁶, A. Onnerstad ¹¹⁷, C. Oppedisano ⁵⁶, A. Ortiz Velasquez ⁶⁵, J. Otwinowski ¹⁰⁷, M. Oya ⁹², K. Oyama ⁷⁶, Y. Pachmayer ⁹⁴, S. Padhan ⁴⁷, D. Pagano ^{134,55}, G. Paic ⁶⁵, S. Paisano-Guzmán ⁴⁴, A. Palasciano ⁵⁰, I. Panasenkov ⁷⁵, S. Panebianco ¹³⁰, C. Pantouvakis ²⁷, H. Park ¹²⁵, H. Park ¹⁰⁴, J. Park ¹²⁵, J.E. Parkkila ³², Y. Patley ⁴⁷, R.N. Patra ⁵⁰, B. Paul ¹³⁵, H. Pei ⁶, T. Peitzmann ⁵⁹, X. Peng ¹¹, M. Pennisi ²⁴, S. Perciballi ²⁴, D. Peresunko ¹⁴⁰, G.M. Perez ⁷, Y. Pestov ¹⁴⁰, M.T. Petersen ⁸³, V. Petrov ¹⁴⁰, M. Petrovici ⁴⁵, S. Piano ⁵⁷, M. Pikna ¹³, P. Pilot ¹⁰³, O. Pinazza ^{51,32}, L. Pinsky ¹¹⁶, C. Pinto ⁹⁵, S. Pisano ⁴⁹, M. Płoskoń ⁷⁴, M. Planinic ⁸⁹, F. Pliquet ⁶⁴, D.K. Plociennik ², M.G. Poghosyan ⁸⁷, B. Polichtchouk ¹⁴⁰, S. Politano ²⁹, N. Poljak ⁸⁹, A. Pop ⁴⁵, S. Porteboeuf-Houssais ¹²⁷, V. Pozdniakov ^{1,141}, I.Y. Pozos ⁴⁴, K.K. Pradhan ⁴⁸, S.K. Prasad ⁴, S. Prasad ⁴⁸, R. Preghenella ⁵¹, F. Prino ⁵⁶, C.A. Pruneau ¹³⁷, I. Pshenichnov ¹⁴⁰, M. Puccio ³², S. Pucillo ²⁴, S. Qiu ⁸⁴, L. Quaglia ²⁴, A.M.K. Radhakrishnan ⁴⁸, S. Ragoni ¹⁴, A. Rai ¹³⁸, A. Rakotozafindrabe ¹³⁰, L. Ramello ^{133,56}, F. Rami ¹²⁹, M. Rasa ²⁶, S.S. Räsänen ⁴³, R. Rath ⁵¹, M.P. Rauch ²⁰, I. Ravasenga ³², K.F. Read ^{87,122}, C. Reckziegel ¹¹², A.R. Redelbach ³⁸, K. Redlich ^{VII,79}, C.A. Reetz ⁹⁷, H.D. Regules-Medel ⁴⁴, A. Rehman ²⁰, F. Reidt ³², H.A. Reme-Ness ³⁴, K. Reygers ⁹⁴, A. Riabov ¹⁴⁰, V. Riabov ¹⁴⁰, R. Ricci ²⁸, M. Richter ²⁰, A.A. Riedel ⁹⁵, W. Riegler ³², A.G. Riffero ²⁴, M. Rignanesi ²⁷,

C. Ripoli ²⁸, C. Ristea ⁶³, M.V. Rodriguez ³², M. Rodríguez Cahuantzi ⁴⁴, S.A. Rodríguez Ramírez ⁴⁴, K. Røed ¹⁹, R. Rogalev ¹⁴⁰, E. Rogochaya ¹⁴¹, T.S. Rogoschinski ⁶⁴, D. Rohr ³², D. Röhrich ²⁰, S. Rojas Torres ³⁵, P.S. Rokita ¹³⁶, G. Romanenko ²⁵, F. Ronchetti ³², E.D. Rosas ⁶⁵, K. Roslon ¹³⁶, A. Rossi ⁵⁴, A. Roy ⁴⁸, S. Roy ⁴⁷, N. Rubini ^{51,25}, J.A. Rudolph ⁸⁴, D. Ruggiano ¹³⁶, R. Rui ²³, P.G. Russek ², R. Russo ⁸⁴, A. Rustomov ⁸¹, E. Ryabinkin ¹⁴⁰, Y. Ryabov ¹⁴⁰, A. Rybicki ¹⁰⁷, J. Ryu ¹⁶, W. Rzeska ¹³⁶, B. Sabiu ⁵¹, S. Sadovsky ¹⁴⁰, J. Saetre ²⁰, K. Šafařík ³⁵, S. Saha ⁸⁰, B. Sahoo ⁴⁸, R. Sahoo ⁴⁸, S. Sahoo ⁶¹, D. Sahu ⁴⁸, P.K. Sahu ⁶¹, J. Saini ¹³⁵, K. Sajdakova ³⁷, S. Sakai ¹²⁵, M.P. Salvan ⁹⁷, S. Sambyal ⁹¹, D. Samitz ¹⁰², I. Sanna ^{32,95}, T.B. Saramela ¹¹⁰, D. Sarkar ⁸³, P. Sarma ⁴¹, V. Sarritzu ²², V.M. Sarti ⁹⁵, M.H.P. Sas ³², S. Sawan ⁸⁰, E. Scapparone ⁵¹, J. Schambach ⁸⁷, H.S. Scheid ⁶⁴, C. Schiaua ⁴⁵, R. Schicker ⁹⁴, F. Schlepper ⁹⁴, A. Schmah ⁹⁷, C. Schmidt ⁹⁷, H.R. Schmidt ⁹³, M.O. Schmidt ³², M. Schmidt ⁹³, N.V. Schmidt ⁸⁷, A.R. Schmier ¹²², R. Schotter ^{102,129}, A. Schröder ³⁸, J. Schukraft ³², K. Schweda ⁹⁷, G. Scioli ²⁵, E. Scomparin ⁵⁶, J.E. Seger ¹⁴, Y. Sekiguchi ¹²⁴, D. Sekihata ¹²⁴, M. Selina ⁸⁴, I. Seluzhenkov ⁹⁷, S. Senyukov ¹²⁹, J.J. Seo ⁹⁴, D. Serebryakov ¹⁴⁰, L. Serkin ⁶⁵, L. Šeršknyte ⁹⁵, A. Sevcenco ⁶³, T.J. Shaba ⁶⁸, A. Shabetai ¹⁰³, R. Shahoyan ³², A. Shangaraev ¹⁴⁰, B. Sharma ⁹¹, D. Sharma ⁴⁷, H. Sharma ⁵⁴, M. Sharma ⁹¹, S. Sharma ⁷⁶, S. Sharma ⁹¹, U. Sharma ⁹¹, A. Shatav ¹³¹, O. Sheibani ¹¹⁶, K. Shigaki ⁹², M. Shimomura ⁷⁷, J. Shin ¹², S. Shirinkin ¹⁴⁰, Q. Shou ³⁹, Y. Sibiriak ¹⁴⁰, S. Siddhanta ⁵², T. Siemiarczuk ⁷⁹, T.F. Silva ¹¹⁰, D. Silvermyr ⁷⁵, T. Simantathammakul ¹⁰⁵, R. Simonov ³⁶, B. Singh ⁹¹, B. Singh ⁹⁵, K. Singh ⁴⁸, R. Singh ⁸⁰, R. Singh ⁹¹, R. Singh ⁹⁷, S. Singh ¹⁵, V.K. Singh ¹³⁵, V. Singhal ¹³⁵, T. Sinha ⁹⁹, B. Sitar ¹³, M. Sitta ^{133,56}, T.B. Skaali ¹⁹, G. Skorodumovs ⁹⁴, N. Smirnov ¹³⁸, R.J.M. Snellings ⁵⁹, E.H. Solheim ¹⁹, J. Song ¹⁶, C. Sonnabend ^{32,97}, J.M. Sonneveld ⁸⁴, F. Soramel ²⁷, A.B. Soto-Hernandez ⁸⁸, R. Spijkers ⁸⁴, I. Sputowska ¹⁰⁷, J. Staa ⁷⁵, J. Stachel ⁹⁴, I. Stan ⁶³, P.J. Steffanic ¹²², T. Stellhorn ¹²⁶, S.F. Stiefelmaier ⁹⁴, D. Stocco ¹⁰³, I. Storehaug ¹⁹, N.J. Strangmann ⁶⁴, P. Stratmann ¹²⁶, S. Strazzi ²⁵, A. Sturmiolo ^{30,53}, C.P. Stylianidis ⁸⁴, A.A.P. Suaide ¹¹⁰, C. Suire ¹³¹, M. Sukhanov ¹⁴⁰, M. Suljic ³², R. Sultanov ¹⁴⁰, V. Sumeria ⁹¹, S. Sumowidagdo ⁸², M. Szymkowski ¹³⁶, S.F. Taghavi ⁹⁵, G. Tailliped ⁹⁷, J. Takahashi ¹¹¹, G.J. Tambave ⁸⁰, S. Tang ⁶, Z. Tang ¹²⁰, J.D. Tapia Takaki ¹¹⁸, N. Tapus ¹¹³, L.A. Tarasovicova ³⁷, M.G. Tazila ⁴⁵, G.F. Tassielli ³¹, A. Tauro ³², A. Tavira García ¹³¹, G. Tejeda Muñoz ⁴⁴, L. Terlizzi ²⁴, C. Terrevoli ⁵⁰, S. Thakur ⁴, D. Thomas ¹⁰⁸, A. Tikhonov ¹⁴⁰, N. Tiltmann ^{32,126}, A.R. Timmins ¹¹⁶, M. Tkacik ¹⁰⁶, T. Tkacik ¹⁰⁶, A. Toia ⁶⁴, R. Tokumoto ⁹², S. Tomassini ²⁵, K. Tomohiro ⁹², N. Topilskaya ¹⁴⁰, M. Toppi ⁴⁹, V.V. Torres ¹⁰³, A.G. Torres Ramos ³¹, A. Trifiró ^{30,53}, T. Triloki ⁹⁶, A.S. Triolo ^{32,30,53}, S. Tripathy ³², T. Tripathy ⁴⁷, S. Trogolo ²⁴, V. Trubnikov ³, W.H. Trzaska ¹¹⁷, T.P. Trzcinski ¹³⁶, C. Tsolanta ¹⁹, R. Tu ³⁹, A. Tumkin ¹⁴⁰, R. Turrisi ⁵⁴, T.S. Tveter ¹⁹, K. Ullaland ²⁰, B. Ulukutlu ⁹⁵, S. Upadhyaya ¹⁰⁷, A. Uras ¹²⁸, M. Urioni ¹³⁴, G.L. Usai ²², M. Vala ³⁷, N. Valle ⁵⁵, L.V.R. van Doremalen ⁵⁹, M. van Leeuwen ⁸⁴, C.A. van Veen ⁹⁴, R.J.G. van Weelden ⁸⁴, P. Vande Vyvre ⁸², D. Varga ⁴⁶, Z. Varga ⁴⁶, P. Vargas Torres ⁶⁵, M. Vasileiou ⁷⁸, A. Vasiliev ^{1,140}, O. Vázquez Doce ⁴⁹, O. Vazquez Rueda ¹¹⁶, V. Vechernin ¹⁴⁰, E. Vercellin ²⁴, S. Vergara Limón ⁴⁴, R. Verma ⁴⁷, L. Vermunt ⁹⁷, R. Vértesi ⁴⁶, M. Verweij ⁵⁹, L. Vickovic ³³, Z. Vilakazi ¹²³, O. Villalobos Baillie ¹⁰⁰, A. Villani ²³, A. Vinogradov ¹⁴⁰, T. Virgili ²⁸, M.M.O. Virta ¹¹⁷, A. Vodopyanov ¹⁴¹, B. Volkel ³², M.A. Völkl ⁹⁴, S.A. Voloshin ¹³⁷, G. Volpe ³¹, B. von Haller ³², I. Vorobyev ³², N. Vozniuk ¹⁴⁰, J. Vrláková ³⁷, J. Wan ³⁹, C. Wang ³⁹, D. Wang ³⁹, Y. Wang ³⁹, Y. Wang ⁶, Z. Wang ³⁹, A. Wegrzynek ³², F.T. Weiglhofer ³⁸, S.C. Wenzel ³², J.P. Wes-

sels ¹²⁶, J. Wiechula ⁶⁴, J. Wikne ¹⁹, G. Wilk ⁷⁹, J. Wilkinson ⁹⁷, G.A. Willems ¹²⁶, B. Windelband ⁹⁴, M. Winn ¹³⁰, J.R. Wright ¹⁰⁸, W. Wu³⁹, Y. Wu ¹²⁰, Z. Xiong¹²⁰, R. Xu ⁶, A. Yadav ⁴², A.K. Yadav ¹³⁵, Y. Yamaguchi ⁹², S. Yang²⁰, S. Yano ⁹², E.R. Yeats¹⁸, Z. Yin ⁶, I.-K. Yoo ¹⁶, J.H. Yoon ⁵⁸, H. Yu¹², S. Yuan²⁰, A. Yuncu ⁹⁴, V. Zaccolo ²³, C. Zampolli ³², F. Zanone ⁹⁴, N. Zardoshti ³², A. Zarochentsev ¹⁴⁰, P. Závada ⁶², N. Zaviyalov¹⁴⁰, M. Zhalov ¹⁴⁰, B. Zhang ^{94,6}, C. Zhang ¹³⁰, L. Zhang ³⁹, M. Zhang ^{127,6}, M. Zhang ⁶, S. Zhang ³⁹, X. Zhang ⁶, Y. Zhang¹²⁰, Z. Zhang ⁶, M. Zhao ¹⁰, V. Zhrebchevskii ¹⁴⁰, Y. Zhi¹⁰, D. Zhou ⁶, Y. Zhou ⁸³, J. Zhu ^{54,6}, S. Zhu¹²⁰, Y. Zhu⁶, S.C. Zugravel ⁵⁶, N. Zurlo ^{134,55}

Affiliation Notes

^I Deceased

^{II} Also at: Max-Planck-Institut für Physik, Munich, Germany

^{III} Also at: Italian National Agency for New Technologies, Energy and Sustainable Economic Development (ENEA), Bologna, Italy

^{IV} Also at: Dipartimento DET del Politecnico di Torino, Turin, Italy

^V Also at: Yildiz Technical University, Istanbul, Türkiye

^{VI} Also at: Department of Applied Physics, Aligarh Muslim University, Aligarh, India

^{VII} Also at: Institute of Theoretical Physics, University of Wrocław, Poland

^{VIII} Also at: An institution covered by a cooperation agreement with CERN

Collaboration Institutes

¹ A.I. Alikhanyan National Science Laboratory (Yerevan Physics Institute) Foundation, Yerevan, Armenia

² AGH University of Krakow, Cracow, Poland

³ Bogolyubov Institute for Theoretical Physics, National Academy of Sciences of Ukraine, Kiev, Ukraine

⁴ Bose Institute, Department of Physics and Centre for Astroparticle Physics and Space Science (CAPSS), Kolkata, India

⁵ California Polytechnic State University, San Luis Obispo, California, United States

⁶ Central China Normal University, Wuhan, China

⁷ Centro de Aplicaciones Tecnológicas y Desarrollo Nuclear (CEADEN), Havana, Cuba

⁸ Centro de Investigación y de Estudios Avanzados (CINVESTAV), Mexico City and Mérida, Mexico

⁹ Chicago State University, Chicago, Illinois, United States

¹⁰ China Institute of Atomic Energy, Beijing, China

¹¹ China University of Geosciences, Wuhan, China

¹² Chungbuk National University, Cheongju, Republic of Korea

¹³ Comenius University Bratislava, Faculty of Mathematics, Physics and Informatics, Bratislava, Slovak Republic

¹⁴ Creighton University, Omaha, Nebraska, United States

¹⁵ Department of Physics, Aligarh Muslim University, Aligarh, India

¹⁶ Department of Physics, Pusan National University, Pusan, Republic of Korea

¹⁷ Department of Physics, Sejong University, Seoul, Republic of Korea

¹⁸ Department of Physics, University of California, Berkeley, California, United States

¹⁹ Department of Physics, University of Oslo, Oslo, Norway

²⁰ Department of Physics and Technology, University of Bergen, Bergen, Norway

²¹ Dipartimento di Fisica, Università di Pavia, Pavia, Italy

²² Dipartimento di Fisica dell'Università and Sezione INFN, Cagliari, Italy

²³ Dipartimento di Fisica dell'Università and Sezione INFN, Trieste, Italy

²⁴ Dipartimento di Fisica dell'Università and Sezione INFN, Turin, Italy

²⁵ Dipartimento di Fisica e Astronomia dell'Università and Sezione INFN, Bologna, Italy

²⁶ Dipartimento di Fisica e Astronomia dell'Università and Sezione INFN, Catania, Italy

²⁷ Dipartimento di Fisica e Astronomia dell'Università and Sezione INFN, Padova, Italy

²⁸ Dipartimento di Fisica 'E.R. Caianiello' dell'Università and Gruppo Collegato INFN, Salerno, Italy

²⁹ Dipartimento DISAT del Politecnico and Sezione INFN, Turin, Italy

³⁰ Dipartimento di Scienze MIFT, Università di Messina, Messina, Italy

³¹ Dipartimento Interateneo di Fisica 'M. Merlin' and Sezione INFN, Bari, Italy

³² European Organization for Nuclear Research (CERN), Geneva, Switzerland

³³ Faculty of Electrical Engineering, Mechanical Engineering and Naval Architecture, University of Split, Split, Croatia

³⁴ Faculty of Engineering and Science, Western Norway University of Applied Sciences, Bergen, Norway

³⁵ Faculty of Nuclear Sciences and Physical Engineering, Czech Technical University in Prague, Prague, Czech Republic

³⁶ Faculty of Physics, Sofia University, Sofia, Bulgaria

³⁷ Faculty of Science, P.J. Šafárik University, Košice, Slovak Republic

³⁸ Frankfurt Institute for Advanced Studies, Johann Wolfgang Goethe-Universität Frankfurt, Frankfurt, Germany

³⁹ Fudan University, Shanghai, China

⁴⁰ Gangneung-Wonju National University, Gangneung, Republic of Korea

⁴¹ Gauhati University, Department of Physics, Guwahati, India

⁴² Helmholtz-Institut für Strahlen- und Kernphysik, Rheinische Friedrich-Wilhelms-Universität Bonn, Bonn, Germany

⁴³ Helsinki Institute of Physics (HIP), Helsinki, Finland

⁴⁴ High Energy Physics Group, Universidad Autónoma de Puebla, Puebla, Mexico

⁴⁵ Horia Hulubei National Institute of Physics and Nuclear Engineering, Bucharest, Romania

⁴⁶ HUN-REN Wigner Research Centre for Physics, Budapest, Hungary

⁴⁷ Indian Institute of Technology Bombay (IIT), Mumbai, India

⁴⁸ Indian Institute of Technology Indore, Indore, India

⁴⁹ INFN, Laboratori Nazionali di Frascati, Frascati, Italy

⁵⁰ INFN, Sezione di Bari, Bari, Italy

⁵¹ INFN, Sezione di Bologna, Bologna, Italy

⁵² INFN, Sezione di Cagliari, Cagliari, Italy

⁵³ INFN, Sezione di Catania, Catania, Italy

⁵⁴ INFN, Sezione di Padova, Padova, Italy

⁵⁵ INFN, Sezione di Pavia, Pavia, Italy

⁵⁶ INFN, Sezione di Torino, Turin, Italy

⁵⁷ INFN, Sezione di Trieste, Trieste, Italy

⁵⁸ Inha University, Incheon, Republic of Korea

⁵⁹ Institute for Gravitational and Subatomic Physics (GRASP), Utrecht University/Nikhef, Utrecht, Netherlands

⁶⁰ Institute of Experimental Physics, Slovak Academy of Sciences, Košice, Slovak Republic

⁶¹ Institute of Physics, Homi Bhabha National Institute, Bhubaneswar, India

⁶² Institute of Physics of the Czech Academy of Sciences, Prague, Czech Republic

⁶³ Institute of Space Science (ISS), Bucharest, Romania

⁶⁴ Institut für Kernphysik, Johann Wolfgang Goethe-Universität Frankfurt, Frankfurt, Germany

⁶⁵ Instituto de Ciencias Nucleares, Universidad Nacional Autónoma de México, Mexico City, Mexico

⁶⁶ Instituto de Física, Universidade Federal do Rio Grande do Sul (UFRGS), Porto Alegre, Brazil

⁶⁷ Instituto de Física, Universidad Nacional Autónoma de México, Mexico City, Mexico

⁶⁸ iThemba LABS, National Research Foundation, Somerset West, South Africa
⁶⁹ Jeonbuk National University, Jeonju, Republic of Korea
⁷⁰ Johann-Wolfgang-Goethe Universität Frankfurt Institut für Informatik, Fachbereich Informatik und Mathematik, Frankfurt, Germany
⁷¹ Korea Institute of Science and Technology Information, Daejeon, Republic of Korea
⁷² KTO Karatay University, Konya, Turkey
⁷³ Laboratoire de Physique Subatomique et de Cosmologie, Université Grenoble-Alpes, CNRS-IN2P3, Grenoble, France
⁷⁴ Lawrence Berkeley National Laboratory, Berkeley, California, United States
⁷⁵ Lund University Department of Physics, Division of Particle Physics, Lund, Sweden
⁷⁶ Nagasaki Institute of Applied Science, Nagasaki, Japan
⁷⁷ Nara Women's University (NWU), Nara, Japan
⁷⁸ National and Kapodistrian University of Athens, School of Science, Department of Physics, Athens, Greece
⁷⁹ National Centre for Nuclear Research, Warsaw, Poland
⁸⁰ National Institute of Science Education and Research, Homi Bhabha National Institute, Jatni, India
⁸¹ National Nuclear Research Center, Baku, Azerbaijan
⁸² National Research and Innovation Agency - BRIN, Jakarta, Indonesia
⁸³ Niels Bohr Institute, University of Copenhagen, Copenhagen, Denmark
⁸⁴ Nikhef, National institute for subatomic physics, Amsterdam, Netherlands
⁸⁵ Nuclear Physics Group, STFC Daresbury Laboratory, Daresbury, United Kingdom
⁸⁶ Nuclear Physics Institute of the Czech Academy of Sciences, Husinec-Řež, Czech Republic
⁸⁷ Oak Ridge National Laboratory, Oak Ridge, Tennessee, United States
⁸⁸ Ohio State University, Columbus, Ohio, United States
⁸⁹ Physics department, Faculty of science, University of Zagreb, Zagreb, Croatia
⁹⁰ Physics Department, Panjab University, Chandigarh, India
⁹¹ Physics Department, University of Jammu, Jammu, India
⁹² Physics Program and International Institute for Sustainability with Knotted Chiral Meta Matter (SKCM2), Hiroshima University, Hiroshima, Japan
⁹³ Physikalisches Institut, Eberhard-Karls-Universität Tübingen, Tübingen, Germany
⁹⁴ Physikalisches Institut, Ruprecht-Karls-Universität Heidelberg, Heidelberg, Germany
⁹⁵ Physik Department, Technische Universität München, Munich, Germany
⁹⁶ Politecnico di Bari and Sezione INFN, Bari, Italy
⁹⁷ Research Division and ExtreMe Matter Institute EMMI, GSI Helmholtzzentrum für Schwerionenforschung GmbH, Darmstadt, Germany
⁹⁸ Saga University, Saga, Japan
⁹⁹ Saha Institute of Nuclear Physics, Homi Bhabha National Institute, Kolkata, India
¹⁰⁰ School of Physics and Astronomy, University of Birmingham, Birmingham, United Kingdom
¹⁰¹ Sección Física, Departamento de Ciencias, Pontificia Universidad Católica del Perú, Lima, Peru
¹⁰² Stefan Meyer Institut für Subatomare Physik (SMI), Vienna, Austria
¹⁰³ SUBATECH, IMT Atlantique, Nantes Université, CNRS-IN2P3, Nantes, France
¹⁰⁴ Sungkyunkwan University, Suwon City, Republic of Korea
¹⁰⁵ Suranaree University of Technology, Nakhon Ratchasima, Thailand
¹⁰⁶ Technical University of Košice, Košice, Slovak Republic
¹⁰⁷ The Henryk Niewodniczanski Institute of Nuclear Physics, Polish Academy of Sciences, Cracow, Poland
¹⁰⁸ The University of Texas at Austin, Austin, Texas, United States

¹⁰⁹ Universidad Autónoma de Sinaloa, Culiacán, Mexico
¹¹⁰ Universidade de São Paulo (USP), São Paulo, Brazil
¹¹¹ Universidade Estadual de Campinas (UNICAMP), Campinas, Brazil
¹¹² Universidade Federal do ABC, Santo Andre, Brazil
¹¹³ Universitatea Nationala de Stiinta si Tehnologie Politehnica Bucuresti, Bucharest, Romania
¹¹⁴ University of Cape Town, Cape Town, South Africa
¹¹⁵ University of Derby, Derby, United Kingdom
¹¹⁶ University of Houston, Houston, Texas, United States
¹¹⁷ University of Jyväskylä, Jyväskylä, Finland
¹¹⁸ University of Kansas, Lawrence, Kansas, United States
¹¹⁹ University of Liverpool, Liverpool, United Kingdom
¹²⁰ University of Science and Technology of China, Hefei, China
¹²¹ University of South-Eastern Norway, Kongsberg, Norway
¹²² University of Tennessee, Knoxville, Tennessee, United States
¹²³ University of the Witwatersrand, Johannesburg, South Africa
¹²⁴ University of Tokyo, Tokyo, Japan
¹²⁵ University of Tsukuba, Tsukuba, Japan
¹²⁶ Universität Münster, Institut für Kernphysik, Münster, Germany
¹²⁷ Université Clermont Auvergne, CNRS/IN2P3, LPC, Clermont-Ferrand, France
¹²⁸ Université de Lyon, CNRS/IN2P3, Institut de Physique des 2 Infinis de Lyon, Lyon, France
¹²⁹ Université de Strasbourg, CNRS, IPHC UMR 7178, F-67000 Strasbourg, France, Strasbourg, France
¹³⁰ Université Paris-Saclay, Centre d'Etudes de Saclay (CEA), IRFU, Département de Physique Nucléaire (DPhN), Saclay, France
¹³¹ Université Paris-Saclay, CNRS/IN2P3, IJCLab, Orsay, France
¹³² Università degli Studi di Foggia, Foggia, Italy
¹³³ Università del Piemonte Orientale, Vercelli, Italy
¹³⁴ Università di Brescia, Brescia, Italy
¹³⁵ Variable Energy Cyclotron Centre, Homi Bhabha National Institute, Kolkata, India
¹³⁶ Warsaw University of Technology, Warsaw, Poland
¹³⁷ Wayne State University, Detroit, Michigan, United States
¹³⁸ Yale University, New Haven, Connecticut, United States
¹³⁹ Yonsei University, Seoul, Republic of Korea
¹⁴⁰ Affiliated with an institute covered by a cooperation agreement with CERN
¹⁴¹ Affiliated with an international laboratory covered by a cooperation agreement with CERN.

References

- [1] S.R. Klein, H. Mäntysaari, Imaging the nucleus with high-energy photons, *Nature Rev. Phys.* 1 (11) (2019) 662–674. [arXiv:1910.10858](https://doi.org/10.1038/s42254-019-0107-6), <https://doi.org/10.1038/s42254-019-0107-6>
- [2] A.J. Baltz, et al., The Physics of Ultraperipheral Collisions at the LHC, *Phys. Rept.* 458 (2008) 1–171. [arXiv:0706.3356](https://doi.org/10.1016/j.physrep.2007.12.001), <https://doi.org/10.1016/j.physrep.2007.12.001>
- [3] C.A. Bertulani, S.R. Klein, J. Nystrand, Physics of ultra-peripheral nuclear collisions, *Ann. Rev. Nucl. Part. Sci.* 55 (2005) 271–310. [arXiv:nucl-ex/0502005](https://doi.org/10.1146/annurev.nucl.55.090704.151526), <https://doi.org/10.1146/annurev.nucl.55.090704.151526>
- [4] S. Acharya, et al., ALICE, First measurement of the $|t|$ -dependence of coherent J/ψ photoproduction, *Phys. Lett. B* 817 (2021) 136280. [arXiv:2101.04623](https://doi.org/10.1016/j.physletb.2021.136280), <https://doi.org/10.1016/j.physletb.2021.136280>
- [5] B. Abelev, et al., ALICE, Coherent J/ψ photoproduction in ultra-peripheral Pb-Pb collisions at $\sqrt{s_{NN}} = 2.76$ TeV, *Phys. Lett. B* 718 (2013) 1273–1283. [arXiv:1209.3715](https://doi.org/10.1016/j.physletb.2012.11.059), <https://doi.org/10.1016/j.physletb.2012.11.059>
- [6] E. Abbas, et al., ALICE, Charmonium and e^+e^- pair photoproduction at mid-rapidity in ultra-peripheral Pb-Pb collisions at $\sqrt{s_{NN}} = 2.76$ TeV, *Eur. Phys. J. C* 73 (11) (2013) 2617. [arXiv:1305.1467](https://doi.org/10.1016/j.physletb.2017.07.001), <https://doi.org/10.1016/j.physletb.2017.07.001>
- [7] V. Khachatryan, et al., CMS, Coherent J/ψ photoproduction in ultra-peripheral PbPb collisions at $\sqrt{s_{NN}} = 2.76$ TeV with the CMS experiment, *Phys. Lett. B* 772 (2017) 489–511. [arXiv:1605.06966](https://doi.org/10.1016/j.physletb.2017.07.001), <https://doi.org/10.1016/j.physletb.2017.07.001>
- [8] S. Acharya, et al., ALICE, Coherent J/ψ photoproduction at forward rapidity in ultra-peripheral Pb-Pb collisions at $\sqrt{s_{NN}} = 5.02$ TeV, *Phys. Lett. B* 798 (2019) 134926. [arXiv:1904.06272](https://doi.org/10.1016/j.physletb.2019.134926), <https://doi.org/10.1016/j.physletb.2019.134926>
- [9] S. Acharya, et al., ALICE, Coherent J/ψ and ψ' photoproduction at midrapidity in ultra-peripheral Pb-Pb collisions at $\sqrt{s_{NN}} = 5.02$ TeV, *Eur. Phys. J. C* 81 (8) (2021) 712. [arXiv:2101.04577](https://doi.org/10.1140/epjc/s10052-021-09437-6), <https://doi.org/10.1140/epjc/s10052-021-09437-6>

- [10] R. Aaij, et al., LHCb, Study of coherent J/ψ production in lead-lead collisions at $\sqrt{s_{NN}} = 5$ TeV, JHEP 07 (2022) 117. [arXiv:2107.03223](https://arxiv.org/abs/2107.03223), [https://doi.org/10.1007/JHEP07\(2022\)117](https://doi.org/10.1007/JHEP07(2022)117)
- [11] S. Acharya, et al., ALICE, Energy dependence of coherent photonuclear production of J/ψ mesons in ultra-peripheral Pb-Pb collisions at $\sqrt{s_{NN}} = 5.02$ TeV, JHEP 10 (2023) 119. [arXiv:2305.19060](https://arxiv.org/abs/2305.19060), [https://doi.org/10.1007/JHEP10\(2023\)119](https://doi.org/10.1007/JHEP10(2023)119)
- [12] A. Tumasyan, et al., CMS, Probing Small Bjorken-x Nuclear Gluonic Structure via Coherent J/ψ Photoproduction in Ultraperipheral Pb-Pb Collisions at $\sqrt{s_{NN}} = 5.02$ TeV, Phys. Rev. Lett. 131 (26) (2023) 262301. [arXiv:2303.16984](https://arxiv.org/abs/2303.16984), <https://doi.org/10.1103/PhysRevLett.131.262301>
- [13] M.I. Abdulhamid, et al., STAR, Observation of Strong Nuclear Suppression in Exclusive J/ψ Photoproduction in Au + Au Ultraperipheral Collisions at RHIC, Phys. Rev. Lett. 133 (5) (2024) 052301. [arXiv:2311.13637](https://arxiv.org/abs/2311.13637), <https://doi.org/10.1103/PhysRevLett.133.052301>
- [14] J. Adam, et al., ALICE, Measurement of an excess in the yield of J/ψ at very low p_T in Pb-Pb collisions at $\sqrt{s_{NN}} = 2.76$ TeV, Phys. Rev. Lett. 116 (22) (2016) 222301. [arXiv:1509.08802](https://arxiv.org/abs/1509.08802), <https://doi.org/10.1103/PhysRevLett.116.222301>
- [15] J. Adam, et al., STAR, Observation of excess J/ψ yield at very low transverse momenta in Au + Au collisions at $\sqrt{s_{NN}} = 200$ GeV and U + U collisions at $\sqrt{s_{NN}} = 193$ GeV, Phys. Rev. Lett. 123 (13) (2019) 132302. [arXiv:1904.11658](https://arxiv.org/abs/1904.11658), <https://doi.org/10.1103/PhysRevLett.123.132302>
- [16] R. Aaij, et al., LHCb, J/ψ photoproduction in Pb-Pb peripheral collisions at $\sqrt{s_{NN}} = 5$ TeV, Phys. Rev. C 105 (3) (2022) L032201. [arXiv:2108.02681](https://arxiv.org/abs/2108.02681), <https://doi.org/10.1103/PhysRevC.105.L032201>
- [17] S. Acharya, et al., ALICE, Photoproduction of low- p_T J/ψ from peripheral to central Pb-Pb collisions at 5.02 TeV, Phys. Lett. B 846 (2023) 137467. [arXiv:2204.10684](https://arxiv.org/abs/2204.10684), <https://doi.org/10.1016/j.physletb.2022.137467>
- [18] M.B. Gay Ducati, S. Martins, Heavy meson photoproduction in peripheral AA collisions, Phys. Rev. D 97 (11) (2018) 116013. [arXiv:1804.09836](https://arxiv.org/abs/1804.09836), <https://doi.org/10.1103/PhysRevD.97.116013>
- [19] J. Cepila, J.G. Contreras, M. Krelina, Coherent and incoherent J/ψ photonuclear production in an energy-dependent hot-spot model, Phys. Rev. C 97 (2) (2018) 024901. [arXiv:1711.01855](https://arxiv.org/abs/1711.01855), <https://doi.org/10.1103/PhysRevC.97.024901>
- [20] W. Zha, S.R. Klein, R. Ma, L. Ruan, T. Todoroki, Z. Tang, Z. Xu, C. Yang, Q. Yang, S. Yang, Coherent J/ψ photoproduction in hadronic heavy-ion collisions, Phys. Rev. C 97 (4) (2018) 044910. [arXiv:1705.01460](https://arxiv.org/abs/1705.01460), <https://doi.org/10.1103/PhysRevC.97.044910>
- [21] W. Zha, L. Ruan, Z. Tang, Z. Xu, S. Yang, Double-slit experiment at fermi scale: coherent photoproduction in heavy-ion collisions, Phys. Rev. C 99 (6) (2019) 061901. [arXiv:1810.10694](https://arxiv.org/abs/1810.10694), <https://doi.org/10.1103/PhysRevC.99.061901>
- [22] M. Khusek-Gawenda, A. Szczurek, Photoproduction of J/ψ mesons in peripheral and semicentral heavy ion collisions, Phys. Rev. C 93 (4) (2016) 044912. [arXiv:1509.03173](https://arxiv.org/abs/1509.03173), <https://doi.org/10.1103/PhysRevC.93.044912>
- [23] W. Shi, W. Zha, B. Chen, Charmonium Coherent Photoproduction and Hadroproduction with Effects of Quark Gluon Plasma, Phys. Lett. B 777 (2018) 399–405. [arXiv:1710.00332](https://arxiv.org/abs/1710.00332), <https://doi.org/10.1016/j.physletb.2017.12.055>
- [24] L. Jenkovszky, V. Libov, M.V.T. Machado, Regge phenomenology and coherent photoproduction of J/ψ in peripheral heavy ion collisions, Phys. Lett. B 827 (2022) 137004. [arXiv:2202.02162](https://arxiv.org/abs/2202.02162), <https://doi.org/10.1016/j.physletb.2022.137004>
- [25] K. Aamodt, et al., ALICE, The ALICE experiment at the CERN LHC, JINST 3 (2008) S08002. <https://doi.org/10.1088/1748-0221/3/08/S08002>
- [26] B.B. Abelev, et al., ALICE, Performance of the ALICE Experiment at the CERN LHC, Int. J. Mod. Phys. A 29 (2014) 1430044. [arXiv:1402.4476](https://arxiv.org/abs/1402.4476), <https://doi.org/10.1142/S0217751X14300440>
- [27] K. Aamodt, et al., ALICE, Alignment of the ALICE Inner Tracking System with cosmic-ray tracks, JINST 5 (2010) P03003. [arXiv:1001.0502](https://arxiv.org/abs/1001.0502) [physics.ins-det] <https://doi.org/10.1088/1748-0221/5/03/P03003>
- [28] J. Alme, et al., The ALICE TPC, a large 3-dimensional tracking device with fast readout for ultra-high multiplicity events, Nucl. Instrum. Meth. A622 (2010) 316–367. [arXiv:1001.1950](https://arxiv.org/abs/1001.1950), <https://doi.org/10.1016/j.nima.2010.04.042>
- [29] E. Abbas, et al., ALICE, Performance of the ALICE VZERO system, JINST 8 (2013) P10016. [arXiv:1306.3130](https://arxiv.org/abs/1306.3130), <https://doi.org/10.1088/1748-0221/8/10/P10016>
- [30] B. Abelev, et al., ALICE, Centrality determination of Pb-Pb collisions at $\sqrt{s_{NN}} = 2.76$ TeV with ALICE, Phys. Rev. C 88 (4) (2013) 044909. [arXiv:1301.4361](https://arxiv.org/abs/1301.4361), <https://doi.org/10.1103/PhysRevC.88.044909>
- [31] R. Arnaldi, et al., The Zero degree calorimeters for the ALICE experiment, Nucl. Instrum. Meth. A 581 (2007) 397–401. [Erratum: Nucl. Instrum. Meth. A 604, 765 (2009)]. <https://doi.org/10.1016/j.nima.2008.04.009>
- [32] S. Acharya, et al., ALICE, ALICE luminosity determination for Pb–Pb collisions at $\sqrt{s_{NN}} = 5.02$ TeV (2021). <https://cds.cern.ch/record/2749127>.
- [33] W. Blum, L. Rolandi, W. Riegler, Particle detection with drift chambers, Particle Acceleration and Detection, Springer, 2008. <https://doi.org/10.1007/978-3-540-76684-1>
- [34] S. Acharya, et al., ALICE, Inclusive J/ψ production at mid-rapidity in pp collisions at $\sqrt{s} = 5.02$ TeV, JHEP 10 (2019) 084. [arXiv:1905.07211](https://arxiv.org/abs/1905.07211), [https://doi.org/10.1007/JHEP10\(2019\)084](https://doi.org/10.1007/JHEP10(2019)084)
- [35] S. Acharya, et al., ALICE, Inclusive J/ψ production at midrapidity in pp collisions at $\sqrt{s} = 13$ TeV, Eur. Phys. J. C 81 (12) (2021) 1121. [arXiv:2108.01906](https://arxiv.org/abs/2108.01906), <https://doi.org/10.1140/epjc/s10052-021-09873-4>
- [36] S. Acharya, et al., ALICE, Centrality and transverse momentum dependence of inclusive J/ψ production at midrapidity in Pb–Pb collisions at $\sqrt{s_{NN}} = 5.02$ TeV, Phys. Lett. B 805 (2020) 135434. [arXiv:1910.14404](https://arxiv.org/abs/1910.14404), <https://doi.org/10.1016/j.physletb.2020.135434>
- [37] S. Acharya, et al., ALICE, Measurements of inclusive J/ψ production at midrapidity and forward rapidity in Pb – Pb collisions at $\sqrt{s_{NN}} = 5.02$ TeV, Phys. Lett. B 849 (2024) 138451. [arXiv:2303.13361](https://arxiv.org/abs/2303.13361), <https://doi.org/10.1016/j.physletb.2024.138451>
- [38] X.-N. Wang, M. Gyulassy, HIJING: A Monte Carlo model for multiple jet production in pp, pA, and AA collisions, Phys. Rev. D 44 (1991) 3501–3516. <https://doi.org/10.1103/PhysRevD.44.3501>
- [39] P. Golonka, Z. Was, PHOTOS Monte Carlo: A Precision tool for QED corrections in Z and W decays, Eur. Phys. J. C 45 (2006) 97–107. [arXiv:hep-ph/0506026](https://arxiv.org/abs/hep-ph/0506026) <https://doi.org/10.1140/epjc/s2005-02396-4>
- [40] R. Brun, F. Bruyant, M. Maire, A.C. McPherson, P. Zanzanini, GEANT 3: User's guide Geant 3.10, Geant 3.11; rev. version, CERN, Geneva, Geneva, 1987. <https://cds.cern.ch/record/1119728>.
- [41] S.R. Klein, J. Nysstrand, J. Seger, Y. Gorunov, J. Butterworth, STARlight: A Monte Carlo simulation program for ultra-peripheral collisions of relativistic ions, Comput. Phys. Commun. 212 (2017) 258–268. [arXiv:1607.03838](https://arxiv.org/abs/1607.03838), <https://doi.org/10.1016/j.cpc.2016.10.016>
- [42] S. Acharya, et al., ALICE, First polarisation measurement of coherently photoproduced J/ψ in ultra-peripheral Pb–Pb collisions at $\sqrt{s_{NN}} = 5.02$ TeV (2023). [arXiv:2304.10928](https://arxiv.org/abs/2304.10928)
- [43] C. Alexa, et al., HI, Elastic and Proton-Dissociative Photoproduction of J/ψ Mesons at HERA, Eur. Phys. J. C 73 (6) (2013) 2466. [arXiv:1304.5162](https://arxiv.org/abs/1304.5162), <https://doi.org/10.1140/epjc/s10052-013-2466-y>
- [44] S. Navas, et al., Particle Data Group, Review of particle physics, Phys. Rev. D 110 (3) (2024) 030001. <https://doi.org/10.1103/PhysRevD.110.030001>
- [45] S. Acharya, et al., ALICE, ALICE luminosity determination for Pb–Pb collisions at $\sqrt{s_{NN}} = 5.02$ TeV, JINST 19 (02) (2024) P02039. [arXiv:2204.10148](https://arxiv.org/abs/2204.10148), <https://doi.org/10.1088/1748-0221/19/02/P02039>
- [46] S. Acharya, et al., ALICE, Centrality determination in heavy ion collisions (2018). ALICE-PUBLIC-2018-011, <https://cds.cern.ch/record/2636623>.
- [47] G. D'Agostini, A Multidimensional unfolding method based on Bayes' theorem, Nucl. Instrum. Meth. A 362 (1995) 487–498. [https://doi.org/10.1016/0168-9002\(95\)00274-X](https://doi.org/10.1016/0168-9002(95)00274-X)
- [48] A. Hocker, V. Kartvelishvili, SVD approach to data unfolding, Nucl. Instrum. Meth. A 372 (1996) 469–481. [arXiv:hep-ph/9509307](https://arxiv.org/abs/hep-ph/9509307), [https://doi.org/10.1016/0168-9002\(95\)01478-0](https://doi.org/10.1016/0168-9002(95)01478-0)
- [49] K.J. Golec-Biernat, M. Wusthoff, Saturation effects in deep inelastic scattering at low Q^2 and its implications on diffraction, Phys. Rev. D 59 (1998) 014017. [arXiv:hep-ph/9807513](https://arxiv.org/abs/hep-ph/9807513), <https://doi.org/10.1103/PhysRevD.59.014017>
- [50] E. Iancu, K. Itakura, S. Munier, Saturation and BFKL dynamics in the HERA data at small x, Phys. Lett. B 590 (2004) 199–208. [arXiv:hep-ph/0310338](https://arxiv.org/abs/hep-ph/0310338), <https://doi.org/10.1016/j.physletb.2004.02.040>
- [51] S. Acharya, et al., ALICE, The ALICE experiment: a journey through QCD, Eur. Phys. J. C 84 (8) (2024) 813. [arXiv:2211.04384](https://arxiv.org/abs/2211.04384), <https://doi.org/10.1140/epjc/s10052-024-12935-y>
- [52] B. Abelev, et al., ALICE, Upgrade of the ALICE Experiment: Letter Of Intent, J. Phys. G 41 (2014) 087001. <https://doi.org/10.1088/0954-3899/41/8/087001>